PHOTOPRODUCTION OF π^0'S FROM PROTONS IN THE FORWARD DIRECTION IN THE REGION OF THE SECOND AND THIRD RESONANCES

Thesis by

Richard Michael Talman

In Partial Fulfillment of the Requirements

For the Degree of

Doctor of Philosophy

California Institute of Technology

Pasadena, California

1963

ACKNOWLEDGEMENTS

This experiment was performed under the supervision of A. V. Tollestrup whose advice and tolerance have been greatly appreciated. R. Gomez has been very helpful and instructive in this and other experiments.

C. R. Clinesmith has been of material help in collecting data, performing and checking calculations, and discussing problems.

Considerable experience was gained in apprenticing to H. Ruderman and M. D. Daybell. Also the author profited from discussions with M. Sands and R. L. Walker. It has been pleasant and valuable to work with all the graduate students.

Time passed in "consultation" with J. Chang, C. Peck, and E. Taylor has been well spent.

The work of L. Loucks and his crew, particularly R. Wileman, and A. Neubieser and the machine operators, has been much appreciated.

Partial financial support of the United States Atomic Energy Commission and the National Research Council of Canada is gratefully acknowledged.

I would like to thank my wife Myrna for moral support.

ABSTRACT

The cross section for photoproduction of neutral pions from protons has been measured at energies near 750, 915 and 1150 Mev and over most of the forward-going π^o C.M. hemisphere. The experimental technique consisted of detecting both of the π^o decay photons with lead glass total absorption counters and, when convenient, the recoil proton with a single scintillation counter. The method is subject to rather large systematic errors but, within these, our results are consistent with other experiments wherever there are overlapping points.

Our data has the striking feature that the cross section is very small at 0^o in the region of the second and third pion nucleon resonances. Also, although the data is not inconsistent with a simple first, second and third resonance model, it appears likely that above the third resonance the pole process consisting of the exchange of a single vector meson is becoming important or even dominant. The evidence at this time mildly suggests that this behaviour is largely due to ω^o mesons and under that hypothesis we are able to estimate some ω^o meson coupling constants. For example, using a prescription of Gell-Mann and Zachariasen, we estimate the partial width for the decay $\omega^o \rightarrow \pi^o + \gamma$ to be 240 Kev.

TABLE OF CONTENTS

APPENDICES

I. INTRODUCTION

In recent years several new heavy mesons have been discovered. Of these, the evidence is indisputable for the ω^o (with mass M equal to 790 Mev, isotopic spin I equal to 0, and spin J equal to 1) (1), the ρ (M = 750 Mev, I = 1, J = 1) (2), and the η (M = 550 Mev, I = 0, J = unknown) (3). Another particle called the ζ (M = 575 Mev, I = 1, J = unknown) has tentatively been "found" (4). Even before these particles were found it had been suggested by many people that the reaction

$$\gamma + p \rightarrow p + \pi^o \qquad (1)$$

might exhibit behaviour demonstrating the influence of J = 1 (vector or pseudo-vector) mesons. This suggestion has been explained by Moravcsik (5). The basic hope was that one could isolate the effects of the "pole" process in which a vector meson (let us always call such a meson X^o) is virtually exchanged as illustrated in the Feynman diagram of Fig. 1. We have measured angular distributions of the reaction (1) and do apparently find observable effects of this pole.

The perturbation method solutions to the field theory of quantum electrodynamics and the weak interaction have been extremely successful. In other words, the correspondence between simple Feynman diagrams and nature is quite faithful when just these processes are involved. On the other hand, when strong interactions are involved the perturbation method becomes not valid as is to be expected since the large coupling constant causes successive terms

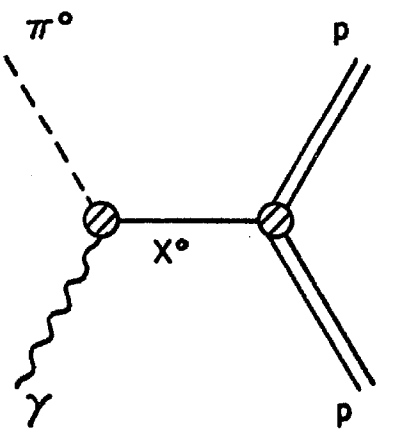

Fig. 1. Feynman diagram for the pole process which this experiment was planned to isolate.

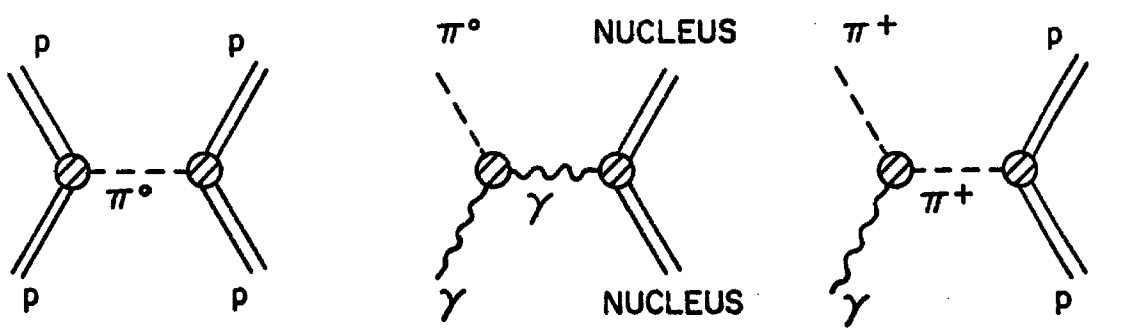

(a) One pion exchange in proton-proton scattering.

(b) Primakoff effect in π° photo-production.

(c) "Retardation" term in π^+ photoproduction.

Fig. 2. Feynman diagram for some important peripheral interactions.

in the perturbation series to grow larger. In spite of this in recent years a kind of phenomenology has grown up in which various strong interaction processes are calculated with considerable success in terms of Feynman diagrams. Feynman (6) himself has emphasized the non-predictive nature of such calculations, since there is often no way of knowing in advance whether or not the supposed simplicity applies to the particular process. For a class of reactions which can be categorized as peripheral, however, Born approximation calculations bear striking resemblances to nature. In an article entitled Practical Utilization of the Nearest Singularity in Dispersion Relations (7) Moravcsik has described some such processes. As examples, we could mention the following: the one pion exchange model of nucleon-nucleon scattering, the importance of the "retardation" term in π^+ photoproduction (one π^+ is exchanged), and the Primakoff effect in π° photoproduction (one γ-ray is exchanged). These are illustrated in Fig. 2.

The success of these calculations in which well known particles are interchanged led us to hope that similar simplicity would show up for processes in which vector mesons can be exchanged. In particular, the process $\gamma + p \to p + \pi^\circ$ is ideal since the requirement that there exist an allowed $\gamma, X^\circ, \pi^\circ$ vertex (see Fig. 1) requires that X° be a neutral, spin 1, particle. This, incidentally, includes the possibility that X° be a photon, in which case the process is the Primakoff process of Fig. 2 (b), but since the effective $\gamma, \gamma, \pi^\circ$ coupling constant is very small (the π° lifetime is long) this process is not expected to be important; this is in spite of the fact that the pole is much closer to the

physical region than the pole with X^o being a massive vector meson.

How do we expect this pole process to show up? Clearly we expect it to affect π^o photoproduction most importantly in the forward-going π^o direction. Rather crudely, the chief effect should be a large ratio of non spin-flip to spin-flip cross section near 0^o. In fact this experiment was partially motivated by the photoproduction measurements from complex nuclei of H. Ruderman et al. (8) which seemed to require that the non spin-flip cross section from hydrogen was large enough at 0^o to be not compatible with the measurements at about 28^o (C.M.) of Berkelman and Waggoner (9) if a single multipole was dominant. Accordingly it was felt to be important to extend the measurements of reaction (1) to 0^o.

In the past, experimental studies of this reaction have relied chiefly on the detection of the recoil proton, with perhaps one of the π^o decay photons being also observed. It was only with extreme effort, however, that Berkelman and Waggoner were able to extend this method to as forward angles as they did. The source of difficulty is the very low energy imparted to the proton in the glancing collision. Accordingly, we have resorted to detecting and measuring the π^o, although, where convenient, we have also detected the recoil proton. The measurements which we are reporting consist of angular distributions at incident photon energies of 750, 915, and 1150 Mev over most of the forward C.M. hemisphere.

The plan of the thesis is as follows. In the body of the thesis we describe all the important features of the experiment as briefly as possible and ignore questions of detail in order to give a continuous and readable account of what has been done. Important

details and calculations are relegated to appendices which are referred to in the text. The appendices are intended to be self-contained with the result that there is a certain amount of repetition. In particular there are no experimental details in the body of the thesis which are not more fully discussed in the appendices.

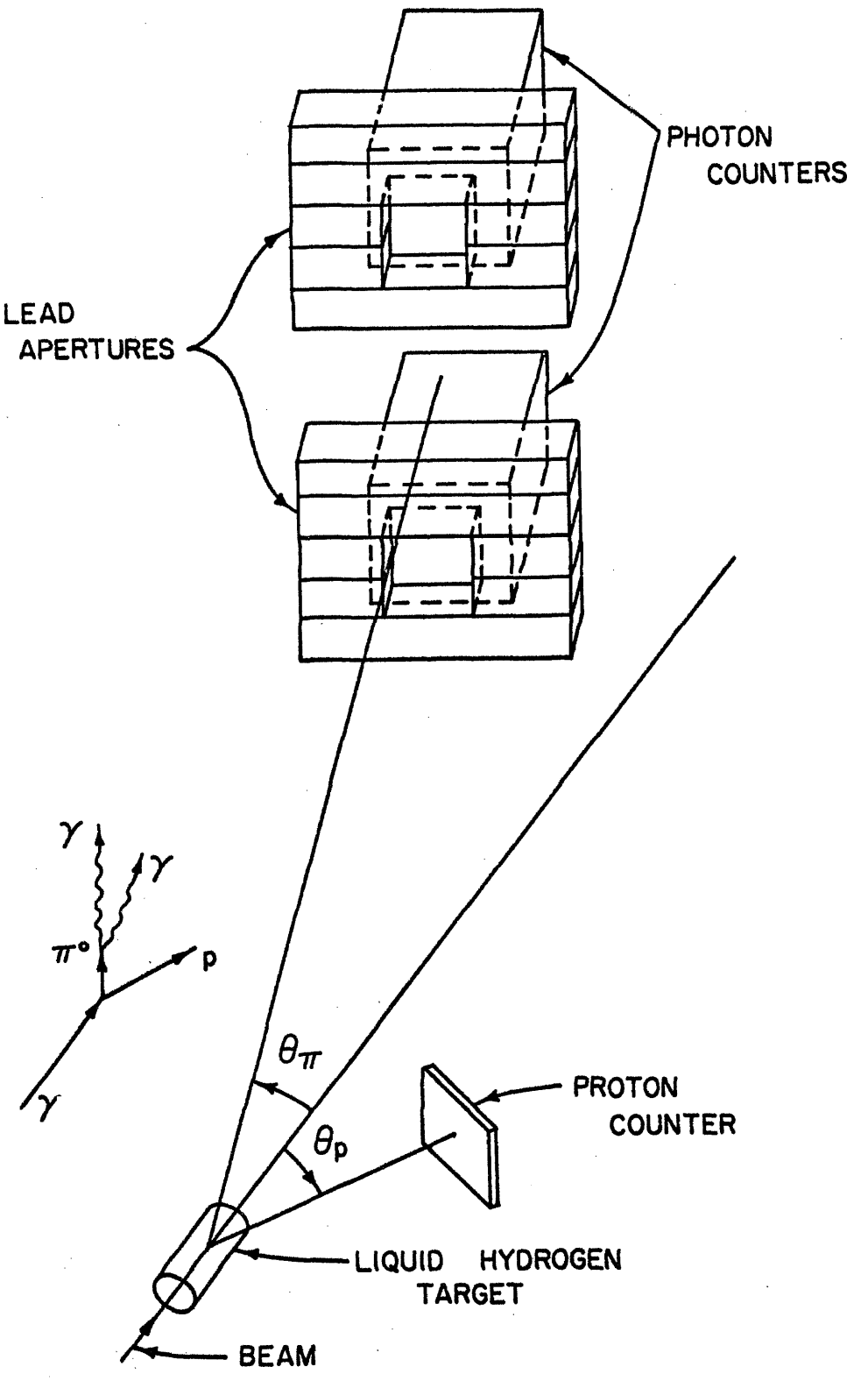

Fig. 3. Perspective view of aparatus when recoil protons were being counted.

II. DESCRIPTION OF THE METHOD

As shown in the introduction it was necessary for us to measure the reaction

$$\gamma + p \rightarrow p + \pi^0$$

by detecting only the π^0. A 16.5cm liquid hydrogen target was placed in the bremsstrahlung beam (which is described in Appendix A) and emergent π^0's were counted as a function of laboratory angle θ_π and incident laboratory photon energy K_L. π^0's were identified by the fast (~15 nsec) coincidence of the pulses from the decay photons in two large total absorption lead glass counters. These counters were energy sensitive, measuring the photon energies to be $K_1 \pm \Delta K_1$ and $K_2 \pm \Delta K_2$ (where ΔK_1 was given by $\frac{\Delta K_1}{K_1} = \frac{0.08}{\sqrt{K_1(Bev)}}$ and similarly for K_2). Apertures in front of these counters were defined as holes in 8" thick lead walls with holes being backed by scintillation counters. These counters vetoed photons which converted in the walls of the aperture as well as rejecting all charged particles. For some wide angle points a scintillation counter was used to count recoil protons. Since this is a two-body process, we could determine the essential kinematical parameters of an individual event by measuring the laboratory angle relative to the beam θ_π and the total laboratory energy E_π. Since π^0's decay into two photons after having gone only a microscopic distance, it was necessary to detect and measure these photons. This was done with a configuration as shown in poor perspective in Fig. 3 and in plan view in Fig. 4. θ_π ($\pm$ a small amount) was given, as shown, in Fig. 3 by the angle of the center of the counters relative to the beam. The most straightforward method of measuring E_π would have been to measure K_1 and K_2.

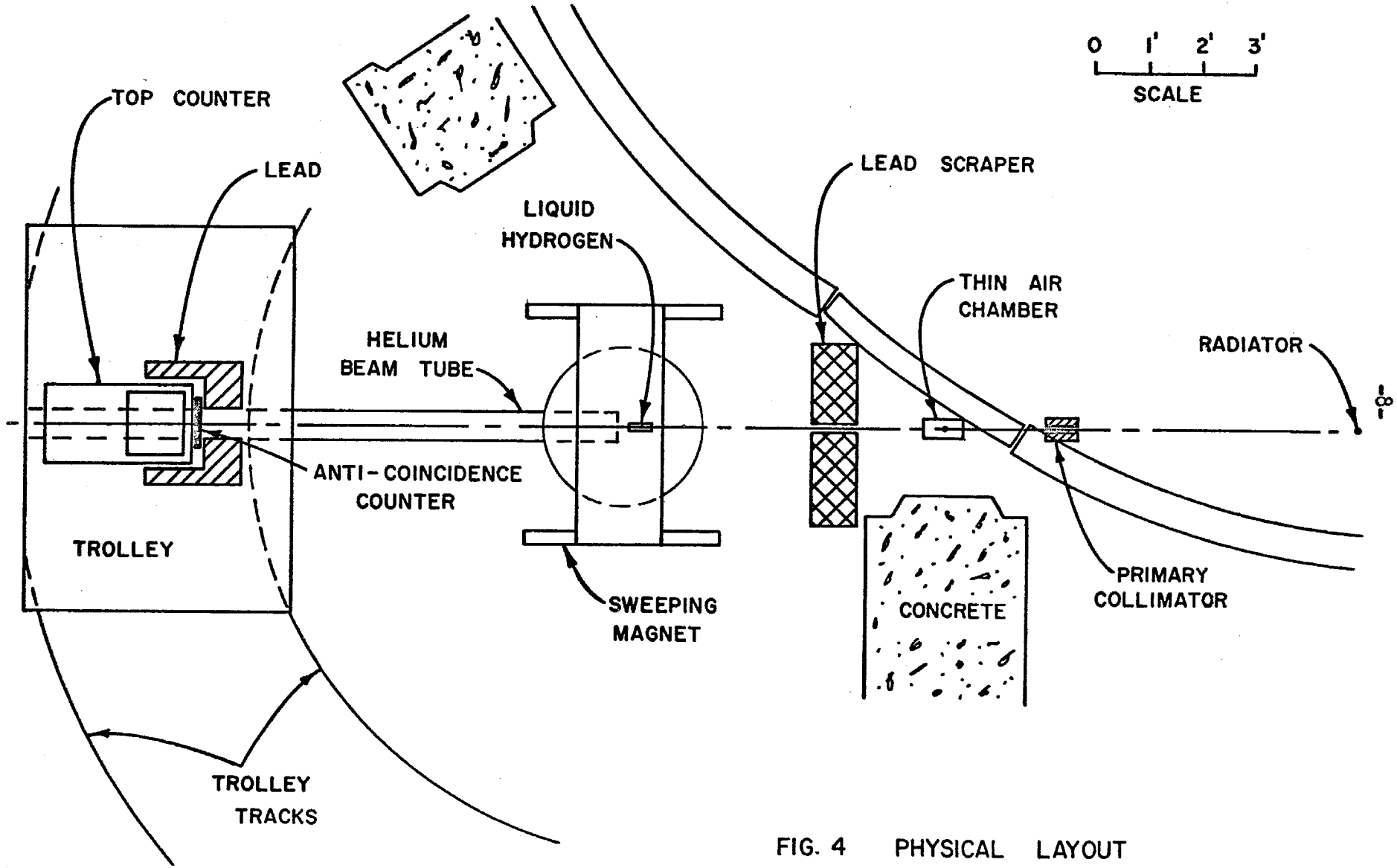

FIG. 4 PHYSICAL LAYOUT

During the actual experiment this was not done (or rather, being done, the information gathered was used only for background rejection and as a consistency check on the experiment). An alternate method, which was followed, of completing the determination of the kinematics was to make use of the opening angle Θ_{π} of the two decay photons to place a lower limit $E_{\pi}(\min)$ on E_{π^0} at the same time letting the bremsstrahlung end point E_0 be an upper limit on K_L. This possibility was based on the property of π^0's that below some minimum E_{π} energy $E_{\pi}(\min)$ the two photon counters were too close to catch both photons of any decay.

In this way we were able to measure π^0 counting rates as a function of laboratory angle. This left just one question: Given a counting rate, what is the cross-section? The solution to this question illustrates many of the fundamental limitations and properties of the method, even apart from backgrounds and other experimental difficulties. Nevertheless, being quite lengthy, it has been relegated to Appendix D. Here we shall mention only enough to aid in the visualization of the experiment. What we require is the analogue of the solid angle-momentum acceptance product of a magnetic spectrometer. For a non-decaying particle this requires a two dimensional integration over particle directions and a one dimensional integration over particle momenta. Since the π^0 decays and we detect both decay particles we must obtain an "effective solid angle"-energy acceptance product which is a seven dimensional integration over counter 1, counter 2, and the π^0 direction and energy. The integrals over the counters give the detection probability for fixed π^0 direction and energy and the effective solid angle is

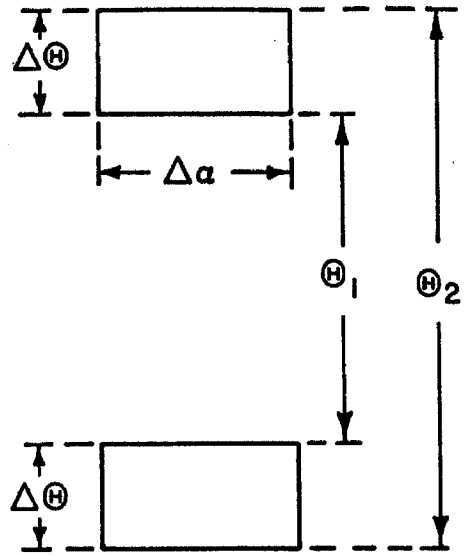

Fig. 5 (a). Schematic view of the counters from the target with the dimensions given as angles subtended at the target.

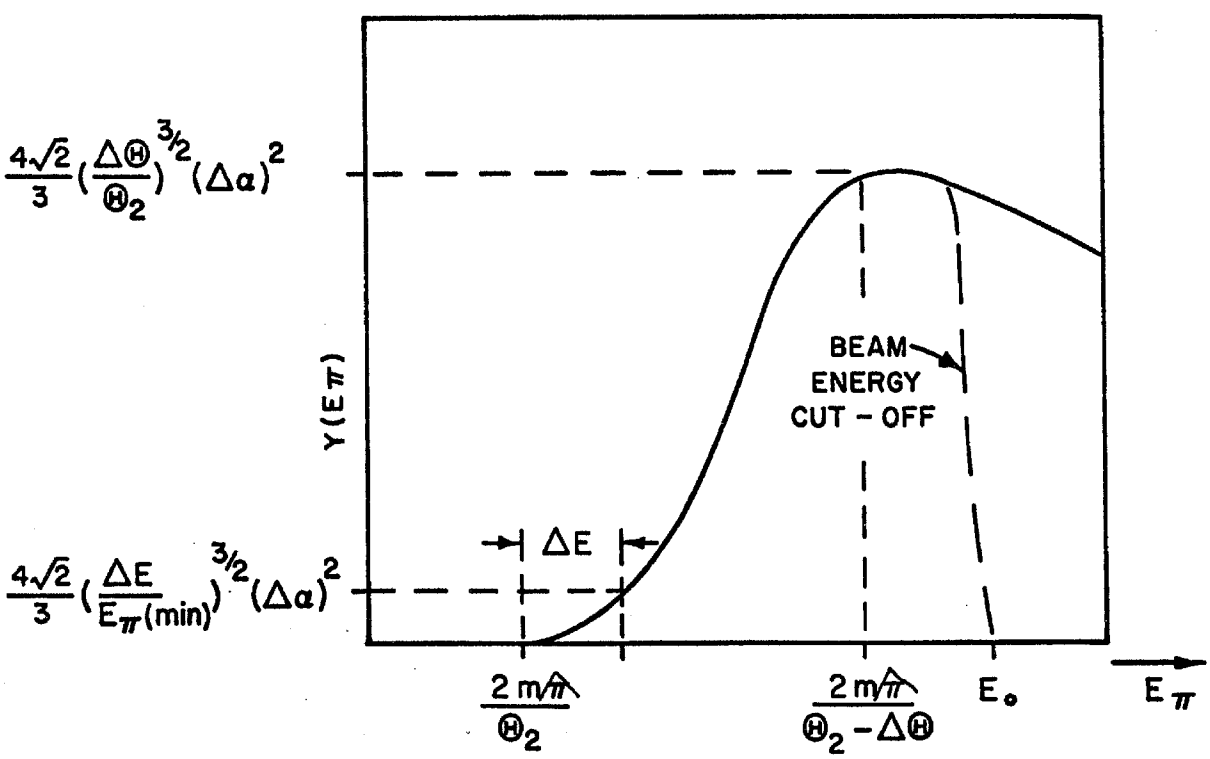

Fig. 5 (b). A graph of $Y(E_\pi)$ for the counter configuration of Fig. 5 (a), showing the orders of magnitude along the axes. It is purely illustrative and is not intended for even crude calculation.

an integral over π^0 directions weighted at each direction by the detection probability, as the name "effective" is meant to imply. The effective solid angle $Y(E_\pi)$ is then the solid angle of a counter which, if the π^0 did not decay, would have the same counting rate as the actual counters, for π^0's of energy E_π.*

The typical shape of $Y(E_\pi)$ is shown in Fig. 5 (b) for the counter configuration shown in Fig. 5 (a). The $K_1 + K_2$ spectrum measured by the photon counters is dominated by $Y(E_\pi)$, being cut off at the upper end corresponding to the beam cut off. Of course this spectrum is also mildly affected by the slow variation of the bremsstrahlung spectrum as well as any energy variation of the cross-section. Neglecting these things as well as the broadening effect of the finite energy resolution of the counters, we can say that the $K_1 + K_2$ spectrum should have the following characteristics:

1) It vanishes below $E_\pi(min) \approx 2m_\pi/\omega_2$.

2) Defining $\Delta E = E_\pi - E_\pi(min)$ the leading edge is given roughly by
$$Y(E_\pi) = \frac{4\sqrt{2}}{3}\left(\frac{\Delta E}{E_\pi(min)}\right)^{3/2}(\Delta\alpha)^2.$$

3) The peak is near $E_\pi = 2m_\pi/(\omega_2 - \Delta\omega)$ after which it slopes down until

4) It is cut off sharply by the bremsstrahlung end point.

---

*It is interesting to note that the typical "effective solid angle"-energy acceptance product of 0.1 Mev-ster in this experiment was of the same order of magnitude as the solid angle momentum acceptance product for the Caltech synchrotron high energy magnet detecting π^+'s of the same energy (1 Bev).

The proportionality factor in fitting the calculated $K_1 + K_2$ spectrum to the measured spectrum gives the cross-section according to the following formula, for incident photon energy K_L,

$$n(E_\pi)\,dE_\pi = \sigma(\theta_\pi(c.m.))\frac{d\Omega(c.m.)}{d\Omega(lab)}\,Y(E_\pi)\,Q\,\frac{B(\hat{k})}{\hat{k}}\,\frac{dk}{dE_\pi}\,\frac{\rho\,\ell_H}{M_p}\,dE_\pi \quad (2)$$

where

$n(E_\pi)$ = number of detected π^0's in a range dE_π at E_π.

$\sigma(\theta_\pi(c.m.))$ = C.M. differential cross-section.

$\frac{d\Omega(c.m.)}{d\Omega(lab)}$ = solid angle transformation from C.M. to lab.

$Y(E_\pi)$ = effective solid angle.

Q = number of equivalent quanta.

$B(\hat{k})$ = bremsstrahlung function defined in Appendix A.

$\hat{k}$ = K/E_0.

ρ = density of liquid hydrogen.

ℓ_H = length of liquid hydrogen.

M_p = mass of one hydrogen atom.

In Fig. 6 the result of such a fit of the calculated to the observed spectrum is shown. The smooth curve was calculated according to equation (2) for the particular counter configuration used while the histogram was observed. Notice that the agreement is good except that there were many coincident γ-ray events which could not have come from π^0's but which could be discarded on the basis of their low $K_1 + K_2$. In Fig. 7 we show several similar histograms to demonstrate that the observed spectra had the same general character at all angles. The slant line in this figure is an empirically chosen bias below which events were discarded and above which they were counted as π^0's. The most important source of the

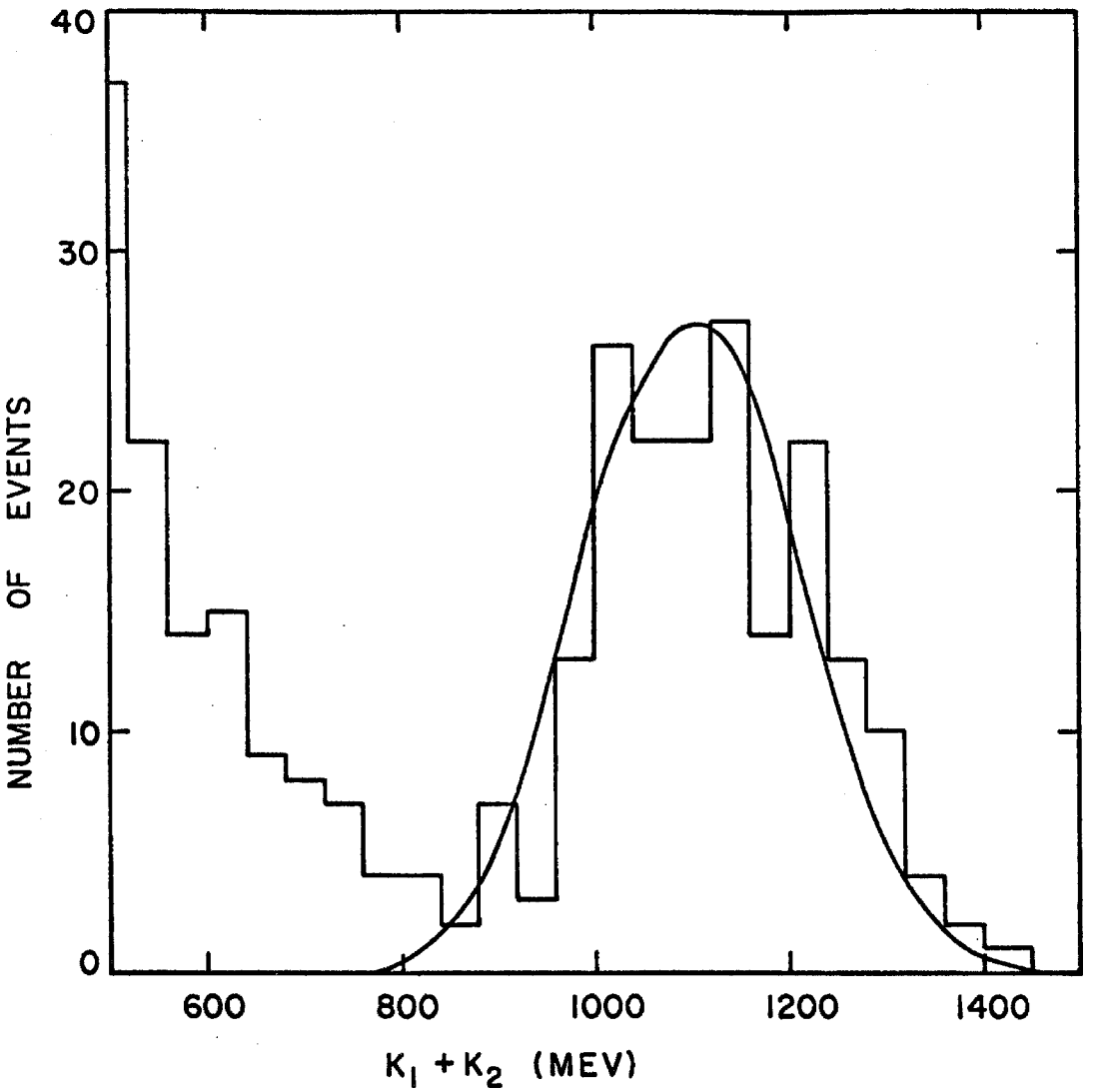

Fig. 5 Spectra of the sum of the energies (K_1 and K_2) of coincident photons for a typical configuration, as measured (histogram) and as expected from π^0's only (smooth curve).

Fig. 7. $K_1 + K_2$ histograms for the series of runs measuring the angular distribution at incident lab photon energy 915 Mev. The numbers indicate the nominal laboratory angle. Empty target backgrounds have been subtracted only from the histograms which have broken lines as their base lines. The slant line indicates the bias below which events were discarded and above which they were called π^o's.

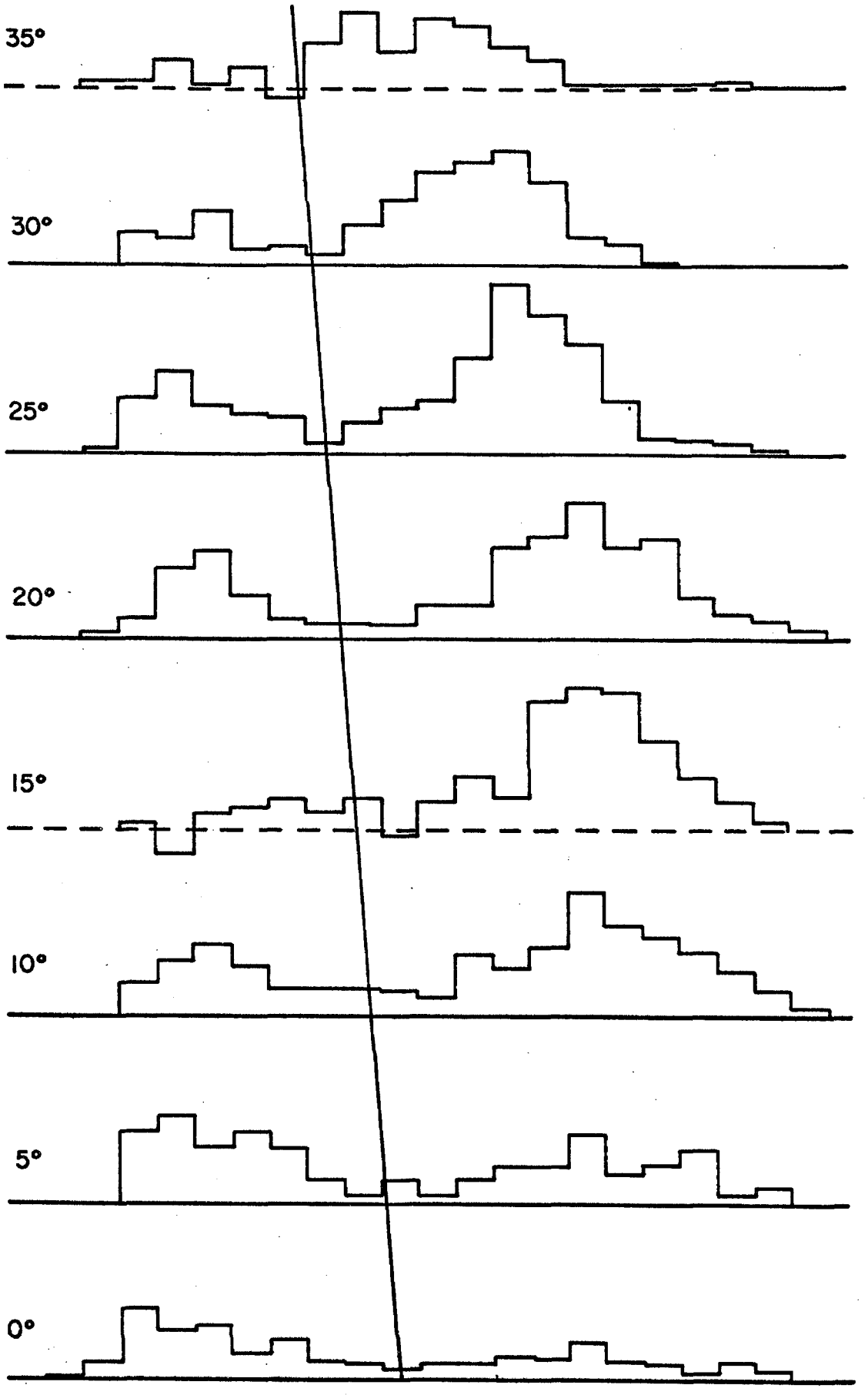
35°
30°
25°
20°
15°
10°
5°
0°

low energy events was probably the reaction

$$\gamma + p \rightarrow p + \pi^0 + \pi^0 \qquad (3)$$

with one γ-ray from each π^0 hitting a counter. Also some of these events were accidentals or individual cosmic rays which went vertically through both counters, but missed the cosmic ray counter.

Various difficulties of an experimental nature were encountered in the course of this experiment. These are extensively discussed in Appendix B. The most important of these were the results of high counting rates in the individual counters. At the most forward angles it was necessary to place the hydrogen target in a magnetic field which swept pair produced electrons away from the counters to reduce these rates. The fast rates resulted in only a negligible number of accidental coincidences simulating π^0's. More serious was the failure to count π^0's because they were in accidental coincidence with pulses in the veto counters. This required a dead time correction which was almost always less than 15% and usually much smaller. (see Appendix B (c) for details)

There were no serious backgrounds and even the empty target backgrounds were small, being about 10% when just the π^0's were detected and about 1% when the recoil proton was also counted. (see Appendix B (d) for details)

Various consistency checks were performed and are described in Appendix B (e). We mention here only the most important of these. We have already seem that the $K_1 + K_2$ spectra were in good agreement with what was expected from single π^0 photoproduction. (Fig. 6). Similarly we could check that, for events which we called

π^{0}'s, the individual K_1 and K_2 distributions were correct or, just as well, the $K_1 - K_2$ spectra. Such a plot is shown in Fig. 8 and the agreement is satisfactory. Another experimental check consisted of leaving the counters fixed and measuring the counting rate as a function of beam energy. The result is shown in Fig. 9 and again the agreement between observation and expectation is satisfactory although it was necessary to assume a 2% discrepancy between the nominal beam energy and the energy calibration determined by this experiment.

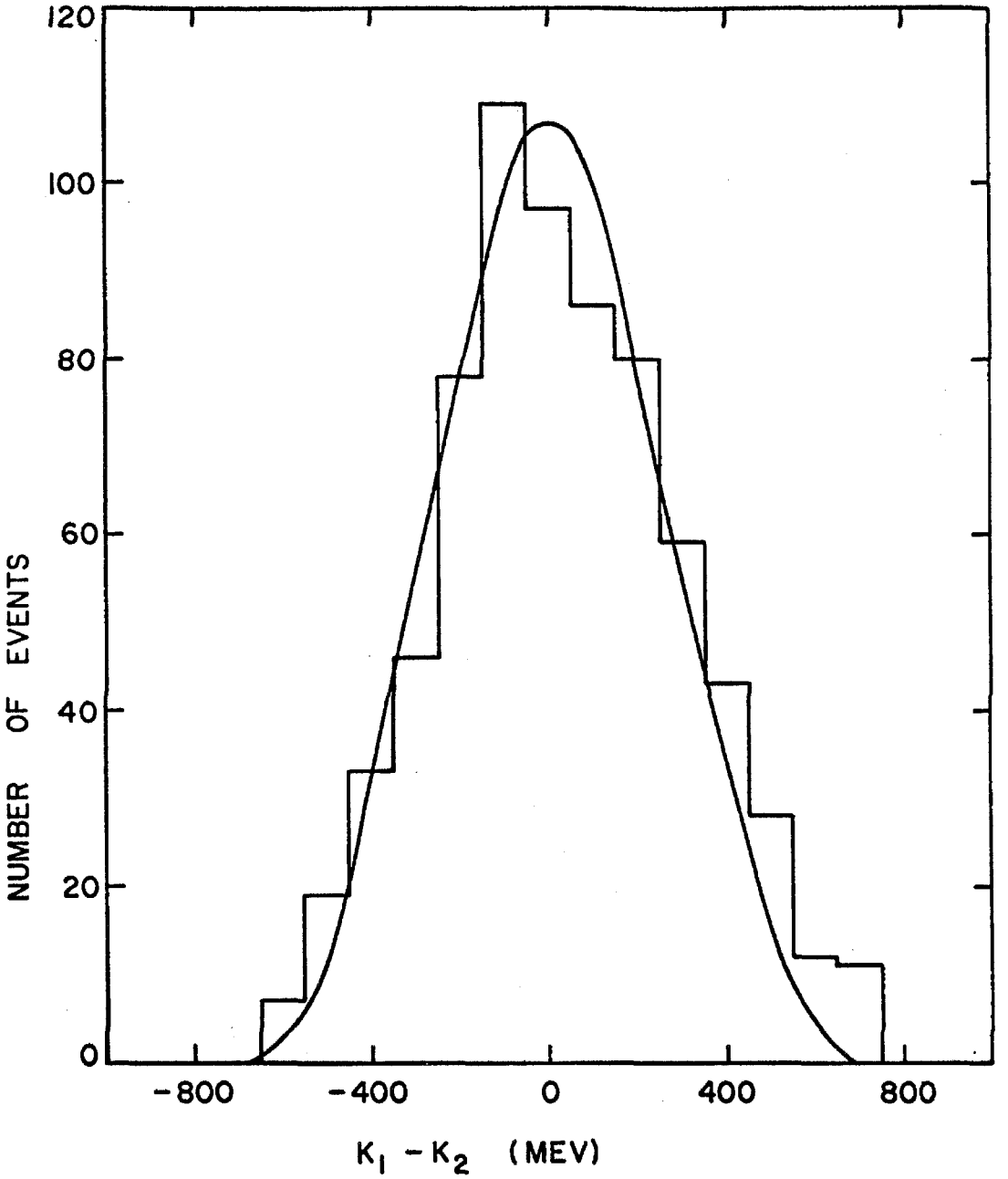

Fig. 8. Typical spectra of the difference of the energies (K_1 and K_2) of coincident photons for which $K_1 + K_2$ was large enough for the event to have been a π^o. The histogram was measured and the smooth curve was calculated.

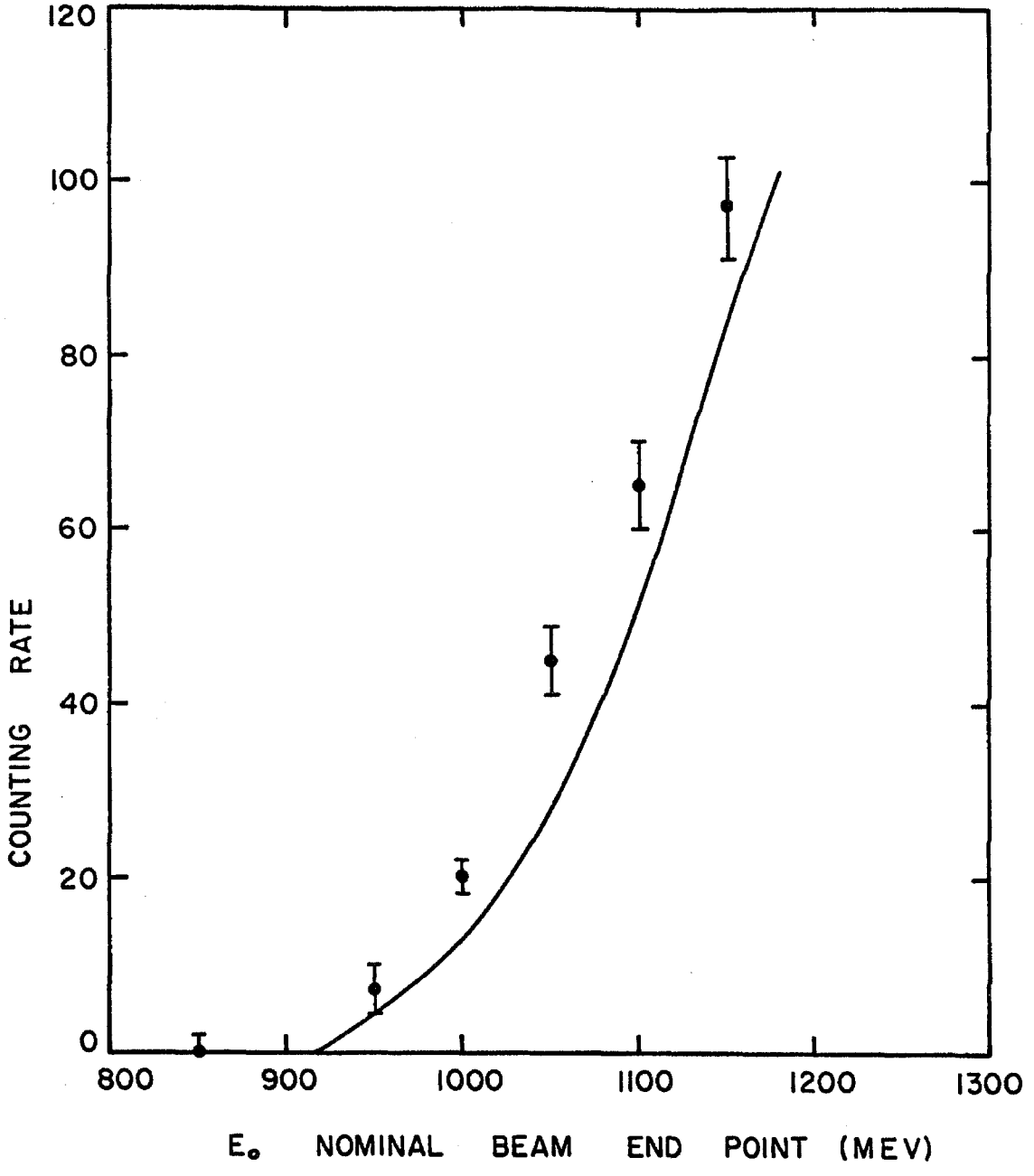

Fig. 9. Resolution Function. For fixed counter configuration the counting rate as a function of the beam end point energy E_0 is shown assuming a constant cross section. This data was interpreted to show that the nominal beam energy disagreed with the energy calibration inherent in this experiment by $2 \pm 1\%$.

III. RESULTS (GRAPHS)

a) General

Our data consists of 5 series of runs which are

(1) An excitation curve at θ_π(C.M.) equal to 50° for incident lab photon energies from 750 Mev to 1200 Mev.

(2)(3) and (4) Angular distributions at incident lab photon energies near 750 Mev, near 915 Mev and near 1150 Mev from 0° to about 60° in the C.M. with just the π^0 being detected.

(5) An angular distribution at incident photon lab energy$_\Lambda$ 1170 Mev from 30° to 100° in the C.M. with protons and π^0's being detected.

The pertinent data for each series is given in Tables 1 to 5. (Appendix C) and the results are given in graphs in Figs. 10 to 13.

It was unfortunate that the central energy was not kept perfectly constant for the angular distributions. It was difficult to do this for a variety of reasons, the most important of which was that the resolution functions were not known at the time the data was taken. Even knowing the resolution functions, a rational method for insuring constant central energies would involve changing the beam energy from angle to angle. That the wide angle data, with protons, was taken near 1170 Mev while the narrow angle data, without protons, was taken near 1150 Mev was the result of the requirement that this experiment be compatible with other experiments taking place at the same time. Note also that for the angular distribution which is nominally near 1150 Mev the energy was as low as 1100 Mev at 0°.

This was a result of the physical impossibility of getting the counters close enough together and still letting the beam through.

These energy shifts were perhaps not too serious since forward of about 40° in the C.M. this experiment would not exclude a cross section independent of energy at fixed angle. This of course was because of the large errors and broad resolution.

Rather wide energy resolution is inherent in this method of measuring π° photoproduction, since the "low energy background" gets relatively worse as the energy resolution is improved. The standard deviation ΔK of the energy resolution function for all points was given approximately by $\Delta K/\bar{K} = 0.06$.

Individual errors were compiled from counting statistics dead time error and the error due to uncertainty in the beam energy. The individual contributions of these errors are shown in Tables 1 to 5. (Appendix C).

In the graphs of Figs. 10 to 13 we plot our results as well as most other results on this reaction at these energies. The points of other experimenters have in some cases been interpolated to give values at the appropriate energies. The same should be done for our points but since, almost within errors, the cross section is flat in energy it was not necessary. In Fig. 13 we have plotted our 50° points as corrected to 60° as well as the 60° points of Diebold et al. (10). This permits an easy comparison.

The cross sections obtained of course depend critically on the calculated efficiencies. These are rather difficult to calculate with the resultant danger of blunders. This danger has been reduced by having two different people perform the calculations

independently and by different methods. The author used an approximate method explained in Appendix D (a) while C.R. Clinesmith performed a Monte Carlo calculation using an IBM 7090, as described in Appendix D (b). The latter calculation was expected to be somewhat more reliable but in fact the two calculations disagreed typically by only 5%. For the series of data taken detecting protons it was necessary to calculate the probability of counting the proton given that a π^o had been counted. This calculation was performed using C.R. Clinesmith's Monte Carlo program and the results are shown in Table 5.

Our estimates of the major systematic errors are 4% due to error in calculating efficiencies, (6% when protons were detected), 5% due to error in the beam end point energy, and 4% due to uncertainty in B ($\hat{K}$). Also presumably constant errors of $+0.04$ μbarns/ster resulted from π -pair contamination and ± 0.10 μbarn/ster from improper discrimination between π^o's and "low energy background."

Fig. 10 C.M. angular distribution of the process $\gamma + p \rightarrow p + \pi^0$ at an incident photon lab energy of 750 Mev. The symbols used in this figure and figures 11 to 13 are identified as follows.

⊙ This experiment, protons not detected.

◎ This experiment, taken from an intersecting series of data and hence useful for checking consistency.

⊗ This experiment, proton detected.

● Vette, (reference 11).

■ Berkelman and Waggoner, (reference 9).

▲ DeWire et al., (reference 12).

▼ Stein and Rogers, (reference 13).

× Worlock et al., (reference 14).

\+ Diebold et al., (reference 10) and Diebold, (reference 36).

✳ Jackson et al., (reference 15).

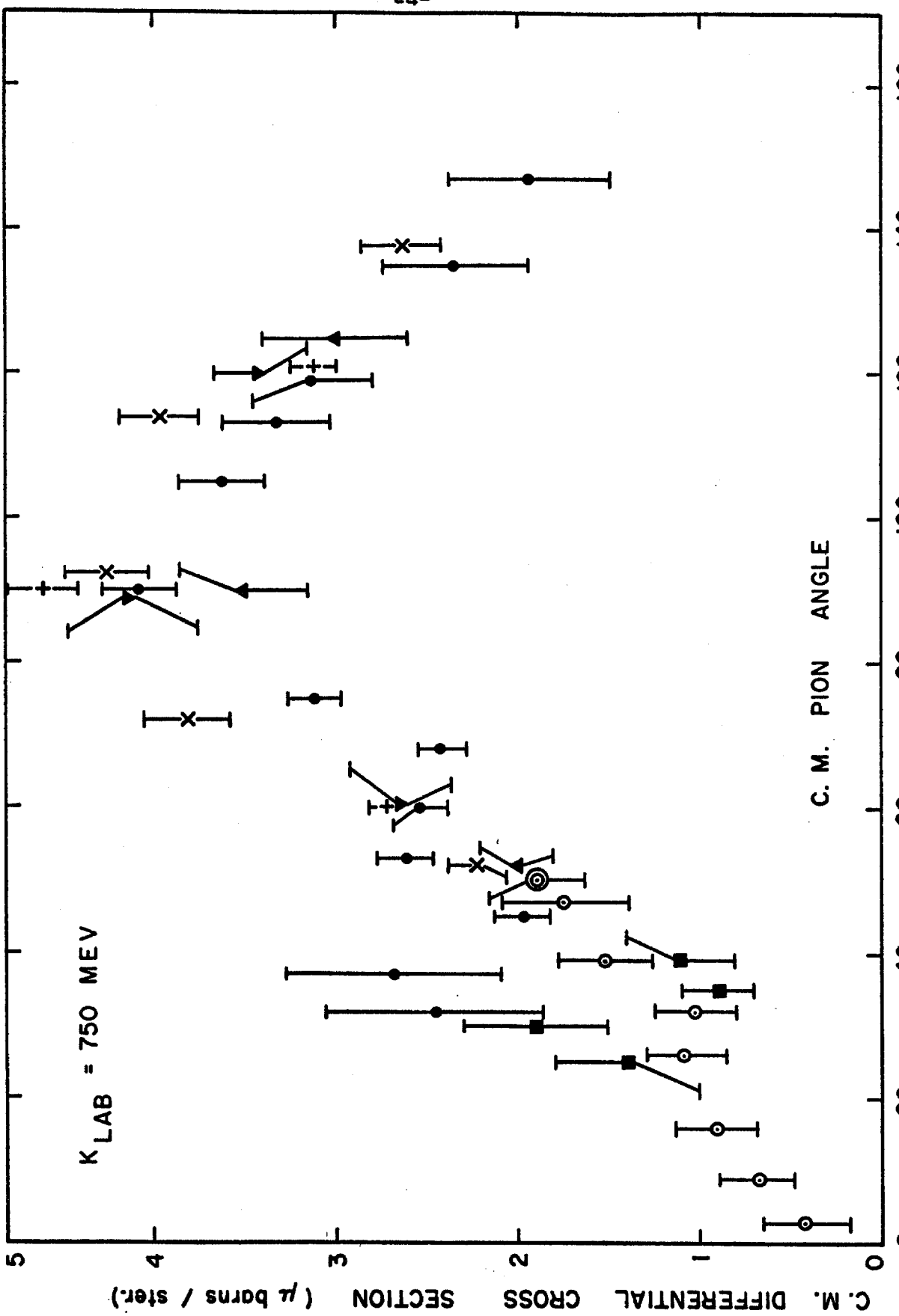
C. M. DIFFERENTIAL CROSS SECTION (μ barns / ster.)
0
1
2
3
4
5
C. M. PION ANGLE
0
20
40
60
80
100
120
140
160
K LAB = 750 MEV

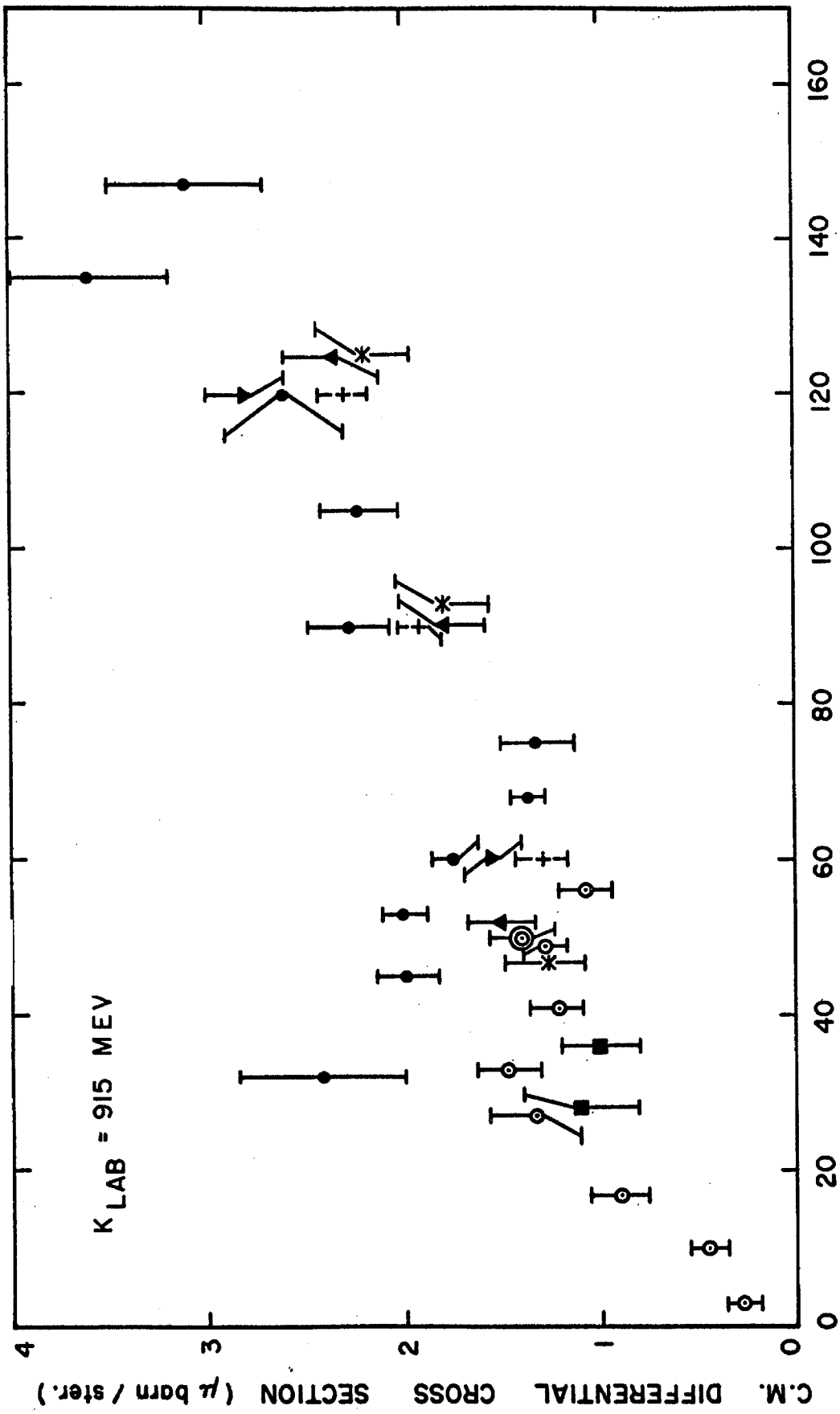

Fig. 11. C.M. angular distribution of the process $\gamma + p \rightarrow p + \pi^0$ at an incident photon lab energy of 915 Mev. For identification of symbols see figure caption to Fig. 10.

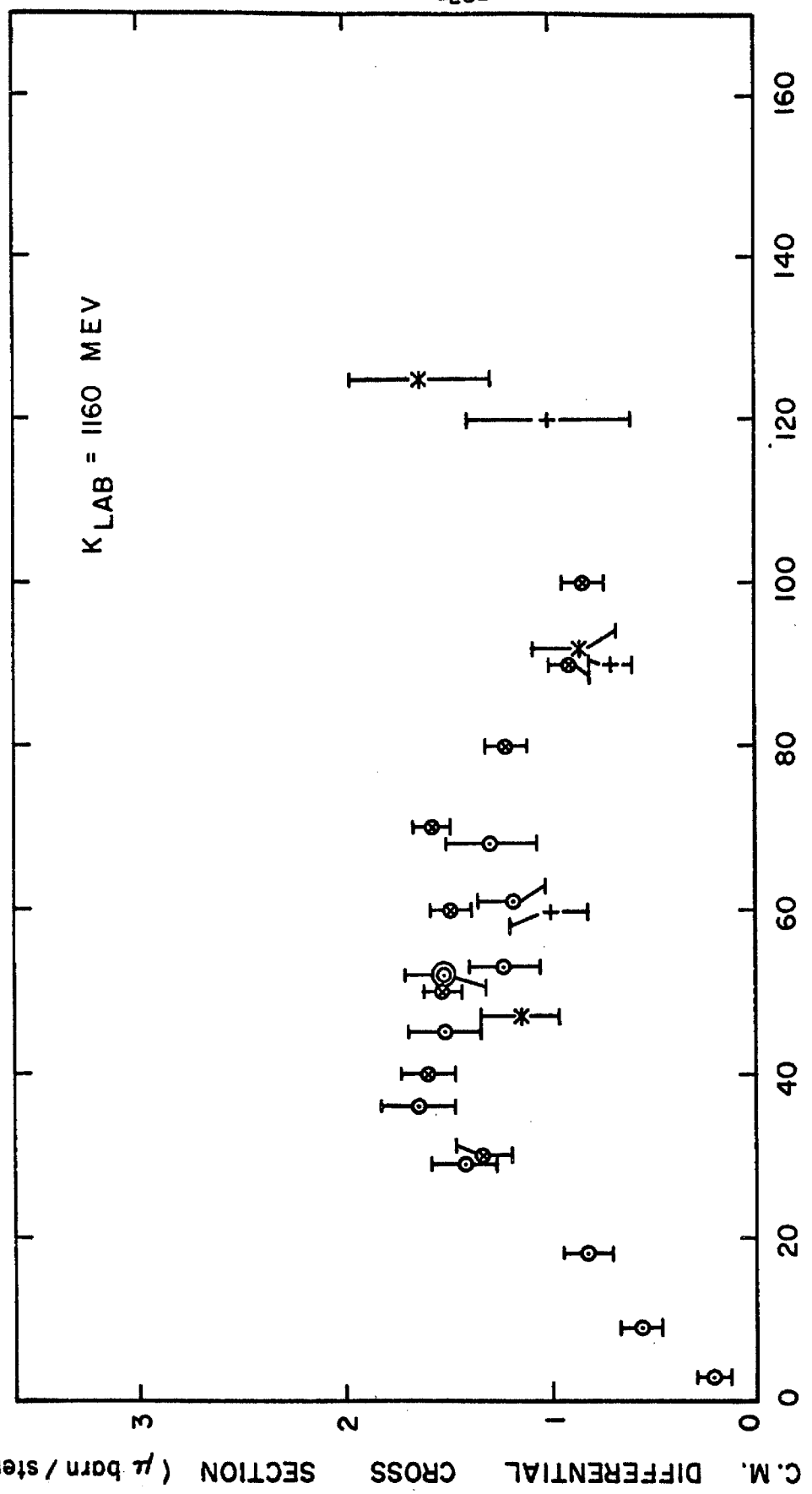

Fig. 12. C.M. angular distribution of the process $\gamma + p \rightarrow p + \pi^0$ at an incident photon lab energy of 1160 Mev. For identification of symbols see figure caption to Fig. 10.

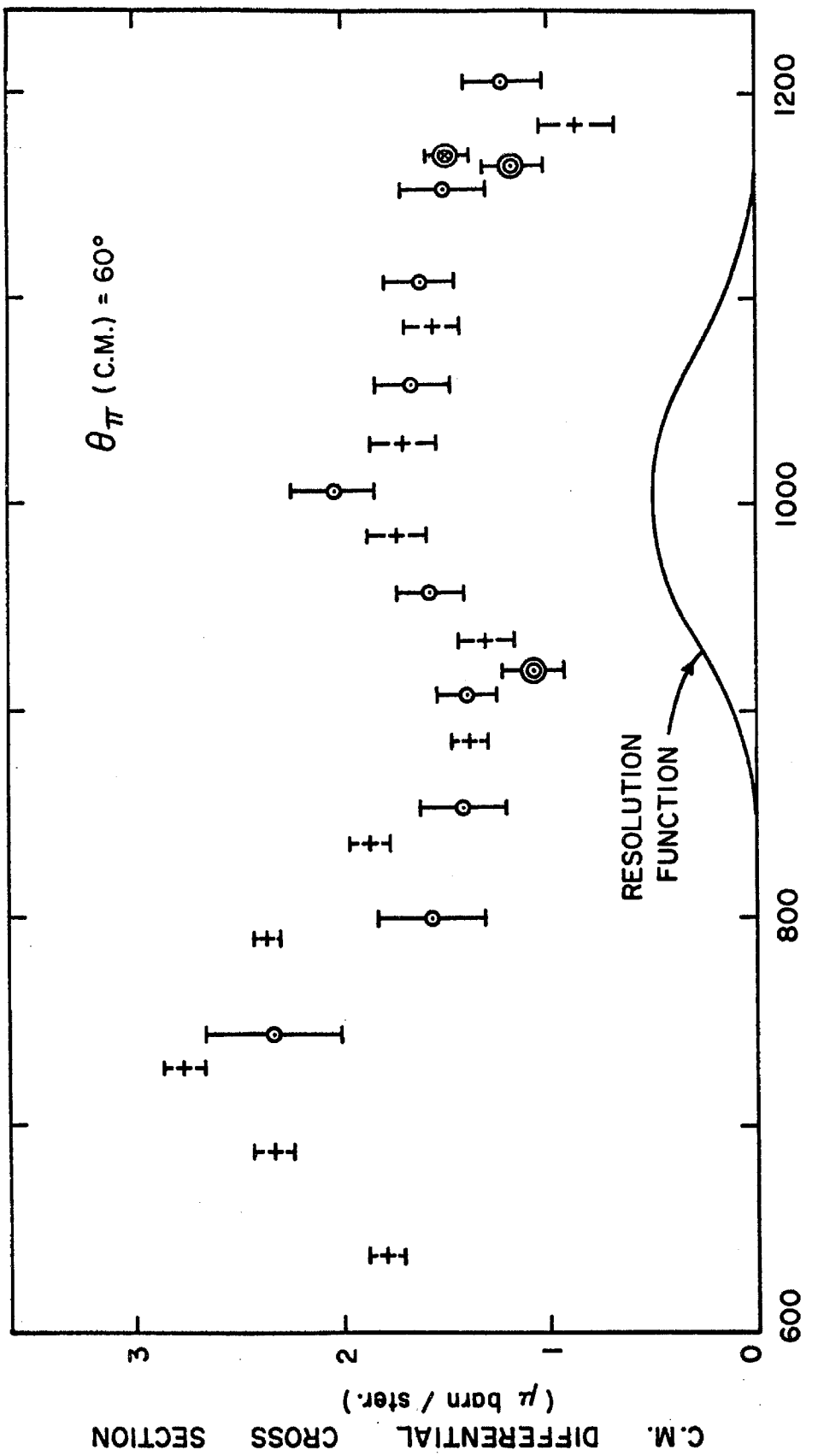

Fig. 13. C.M. cross section vs. incident laboratory photon energy at a C.M. pion angle of 60°. The single circles are data taken at 50° and shifted according to the slope of the cross section. The crosses are data of Diebold (reference 10). The double circles are points measured at 60° in this experiment.

IV. INTERPRETATION

Our aim in performing this experiment was to extract the contribution of a vector meson exchange pole. (Fig. 1) As shown in Appendix E the cross section from this process is approximately given by

$$\frac{d\sigma}{d\Omega} \approx \Gamma(X^\circ \to \pi^\circ + \gamma)\left(\gamma_{XNN}^2/4\pi\right)\frac{9}{M_X^3}\,\frac{\sin^2\theta}{(\cos\theta - \cos\theta_o)^2} \qquad (4)$$

where $\Gamma(X^\circ \to \pi^\circ + \gamma)$ is the partial decay width for the decay $X^\circ \to \pi^\circ + \gamma$ and γ_{XNN} is the coupling constant at the X°, N, N vertex. θ_o is the unphysical angle at which the denominator vanishes and M_X is the mass of the X° meson. The approximation in equation (4) breaks down in the backward hemisphere. For the exact expression see Appendix E. In Fig. 14 we plot the cross section corresponding to the pole alone for M_X = 550 Mev and 790 Mev and for incident photon energies of K_L = 780, 940, and 1180 Mev. The simplest situation which could exist would have this pole process completely dominating the cross section. In that case one could determine M_X from the shape of the cross section. For example at K_L = 1180 Mev, if the cross section were peaked at 58° then the mass of the interchanged vector meson would be 790 Mev. It is clear, however, that the contribution of the pole process is rather insensitive to the mass of the vector meson M_X and that a small contribution from other processes could simulate a mass shift.

Before continuing to the problem of extracting the pole contribution let us consider the data which for convenience has been replotted in Fig. 15 with the abscissa being $x = \cos\theta$.

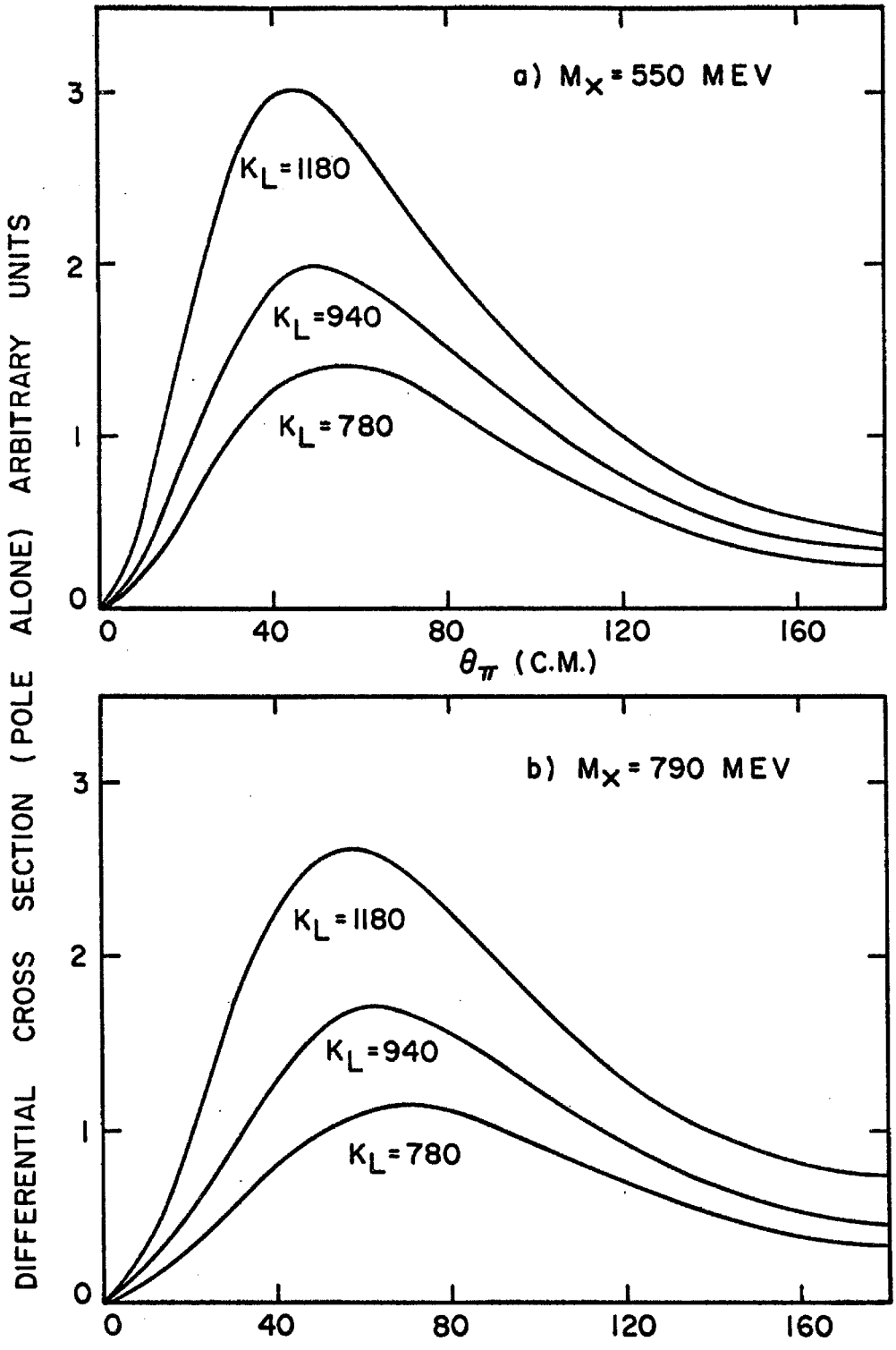

Fig. 14. Angular distributions which would result if the pole process completely dominated π^o photoproduction.

Fig. 15. Differential cross sections for the reaction $\gamma + p \rightarrow p + \pi^0$. The broken lines represent limits within which most earlier measurements lie. The smooth curves are one parameter least squares fits as described in the text. Note the expanded scale of (c).

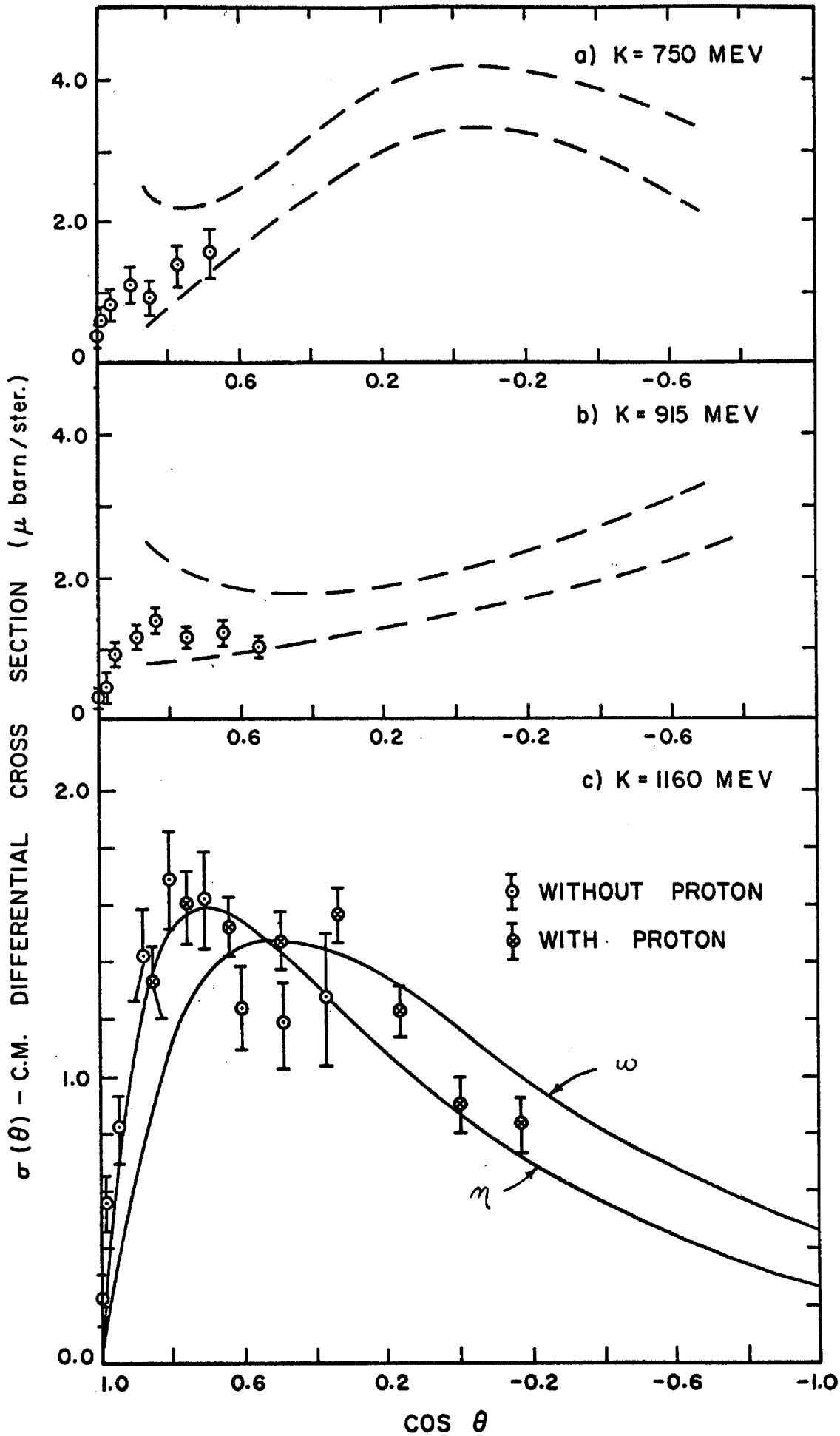
a) K = 750 MEV
b) K = 915 MEV
c) K = 1160 MEV
WITHOUT PROTON
WITH PROTON
ω
η
σ (θ) - C.M. DIFFERENTIAL CROSS SECTION (μ barn / ster.)
COS θ
4.0
2.0
0
1.0
0.0
0.6
0.2
-0.2
-0.6
1.0
-1.0

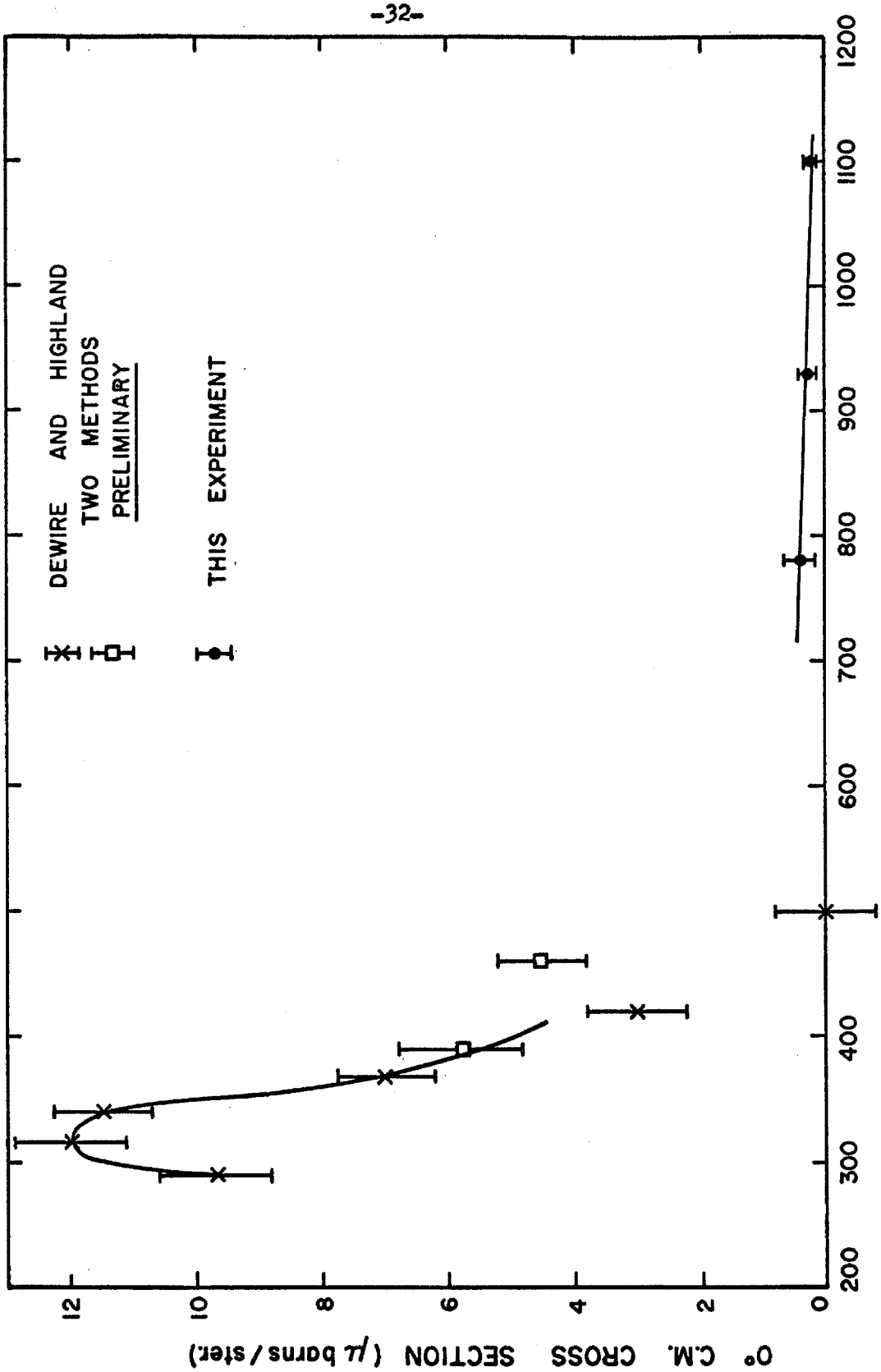

Fig. 15-1. 0° Cross sections for $\gamma + p \rightarrow p + \pi^{0}$. DeWire and Highland emphasize that particularly the 500 Mev point is preliminary and will be repeated.

Surely the most striking feature of the cross section is that it is small in the forward direction, independent of energy. This, incidentally, is not the case at the first resonance ($K_L \approx 375$ Mev) where Highland and Dewire (16) find the 0° cross section to be about 10 μbarns/ster which is in agreement with the usual picture of the first resonance (17). However, preliminary measurements of Highland and Dewire (18) indicate that at $K_L \approx 500$ Mev the 0° cross section has dropped to 0 ± 0.8 μbarns and we find that it stays small at higher energies. In Fig. 15.1 we plot the known 0° cross sections.

This behaviour of the cross section at 0° is interesting for two reasons. First, no single multipole state is particularly small at 0°. Any two multipole states can be combined to give a zero cross section at 0° but one might expect such a cancellation to occur at only a single energy since the phases and magnitudes of the two resonances presumably vary independently according to some resonance formula. This probably means that in the region of the second and third resonances more than two multipoles are important at every energy. Second, π^+ photoproduction from protons is completely different in character and in fact tends to be large at 0° at all energies. It is perhaps only a coincidence that this behaviour of π° and π^+ photoproduction at 0° is consistent with the first order Born approximation which predicts that π° cross sections should be zero at 0° and π^+ cross sections should be large there.

Another striking feature of the data is that at the highest energy we have measured which is above the third resonance the cross section looks a great deal like the cross section expected from a vector meson pole alone. This is illustrated by the smooth

curves of Fig. 15 (c) which are one parameter least squares fits to the data assuming complete dominance of the vector meson pole. For the curve marked ω^o the mass of the exchanged meson was taken to be 790 Mev while for the curve marked η the mass was 550 Mev.

If we take this as showing the existence of such a pole, we are left with the problem of determining which vector mesons are contributing. The situation is still too complicated to proceed rigorously but, partly for illustrative purposes, we investigate the hypothesis that the ω^o exchange pole dominates the cross section above the third resonance. In support of this hypothesis we make the following comments. The evidence for the ζ is somewhat tentative (4). Recent evidence[35] indicates that η can probably decay into 2 γ-rays and hence cannot have spin 1. This leaves only ω^o and ρ^o. Evidence of Ruderman et al. (8) on the coherent production of π^o's from complex nuclei indicates that at least a large portion of the pole-like behaviour which we observe comes from the exchange of a T = 0 vector meson*. Also in the unitary symmetry scheme of Gell-Mann (19) the cross section with ω^o exchanged is expected to be 3 times as large as that with the ρ^o exchanged.

---

*The amplitudes for photoproducing a π^o from a proton and from a neutron are equal when a T = 0 vector meson is virtually exchanged, while they are equal, but of opposite sign, when a T = 1 meson is exchanged. Hence, in the former case, but not in the latter, this process results in a large coherent production near 0^o from complex nuclei. Such an enhancement is indeed observed. While this could arise from any process having a large non-spin flip cross section near 0^o and being constructive from neutrons and protons, the magnitude is roughly correct to correspond to our measurement from protons, if the exchanged meson has T = 0. Unfortunately, a precise comparison is difficult because of the nuclear physics involved.

From equation (4) it is clear that under our hypothesis we can obtain a value for the product of the coupling constants $\Gamma(\omega^0 \to \pi^0 + \gamma)(\gamma_{\omega NN}^2/4\pi)$. We have done this, following Moravcsik (5) by making least squares fits to the data multiplied by $(\cos\theta - \cos\theta_0)^2$ and extrapolating to the pole. As fitting functions we pick first the pole alone, then pole + A_0, then pole + $A_0 + A_1 \cos\theta$ and so on. The results are shown in Fig. 16 which is explained in the figure caption. This plot is similar to those used by Moravcsik and error assignment and the statistical parameter ρ^2 are discussed by him. In Fig. 17 we plot the extrapolations in various orders.

From this plot it is evident that the data is not accurate enough to make our hypothesis more than plausible since it might be argued that terms as high as $\cos^6\theta$ should be present and that gives far too many parameters to be determined by the data. Our data does seem to require higher powers than $\cos^3\theta$ since the points between $x = 0.9$ and $x = 0.7$ seem to be systematically higher than any of the fits obtained. This discrepancy, however, is only of the same order of magnitude as systematic errors known to be present. This curve more than any other should motivate future attempts to perform this experiment more precisely and at higher energies.

There have been efforts by R.E. Diebold and J.R. Kilner to fit all the available pion photoproduction data in the region of the second and third resonance in terms of simple multipoles and Born approximation terms and with no vector meson poles. No coherent overall success has been obtained in following this path, but it has been found possible to fit the reaction

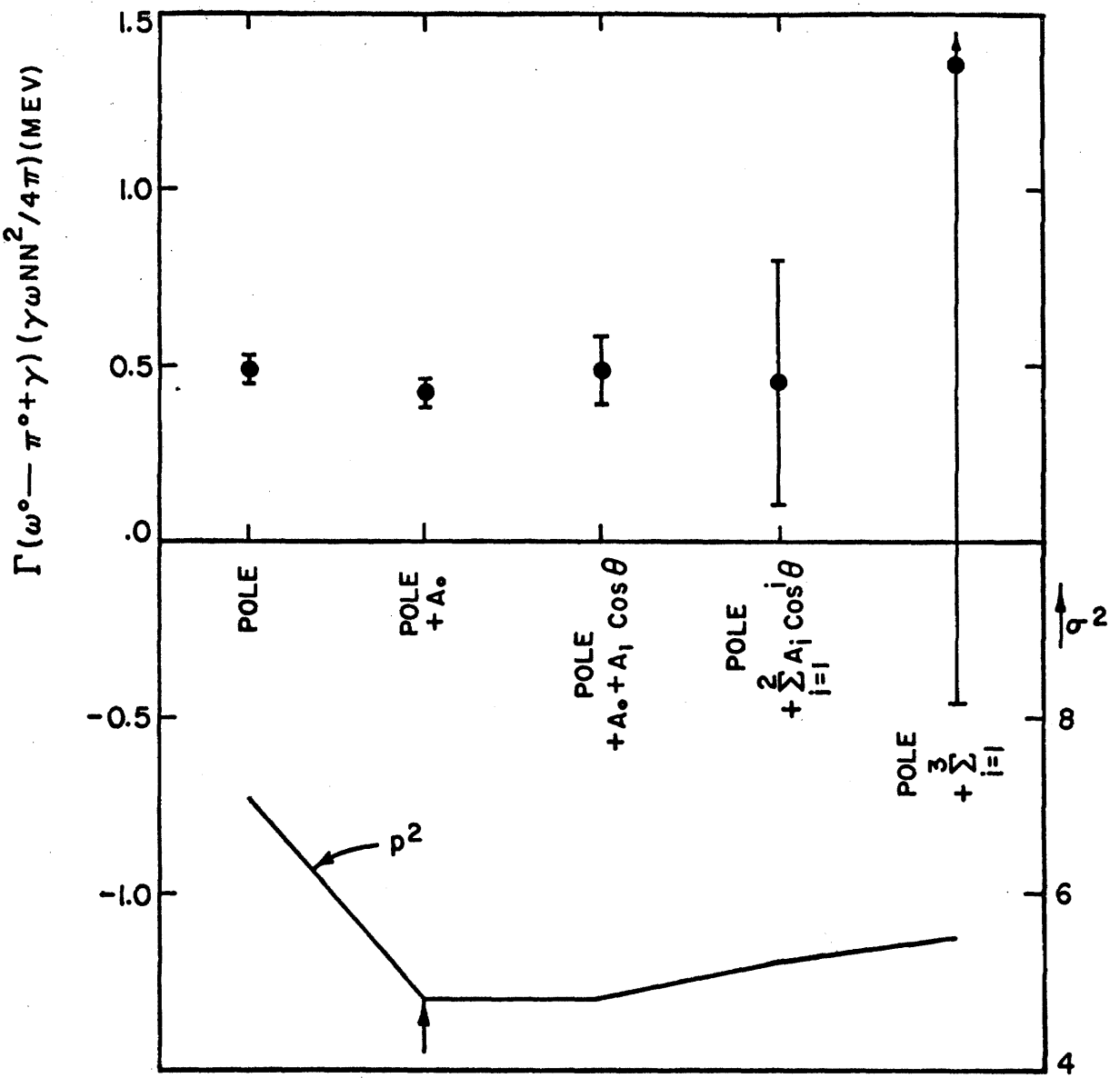

Fig. 16. Plot showing the coupling constants determined in extrapolating a series of fitting functions. The statistical parameter ρ^2 should be about 1 for a good fit if the data were statistically distributed with the quoted errors but systematic discrepancies between the sets of data used invalidated the statistical interpretation of ρ^2. Our interpretation of ρ^2 is that a qualitatively good fit to this particular data will have ρ^2 near 5. Moravscik's prescription is to accept the first fit at which ρ^2 begins its gradual increase. This point is indicated by a vertical arrow.

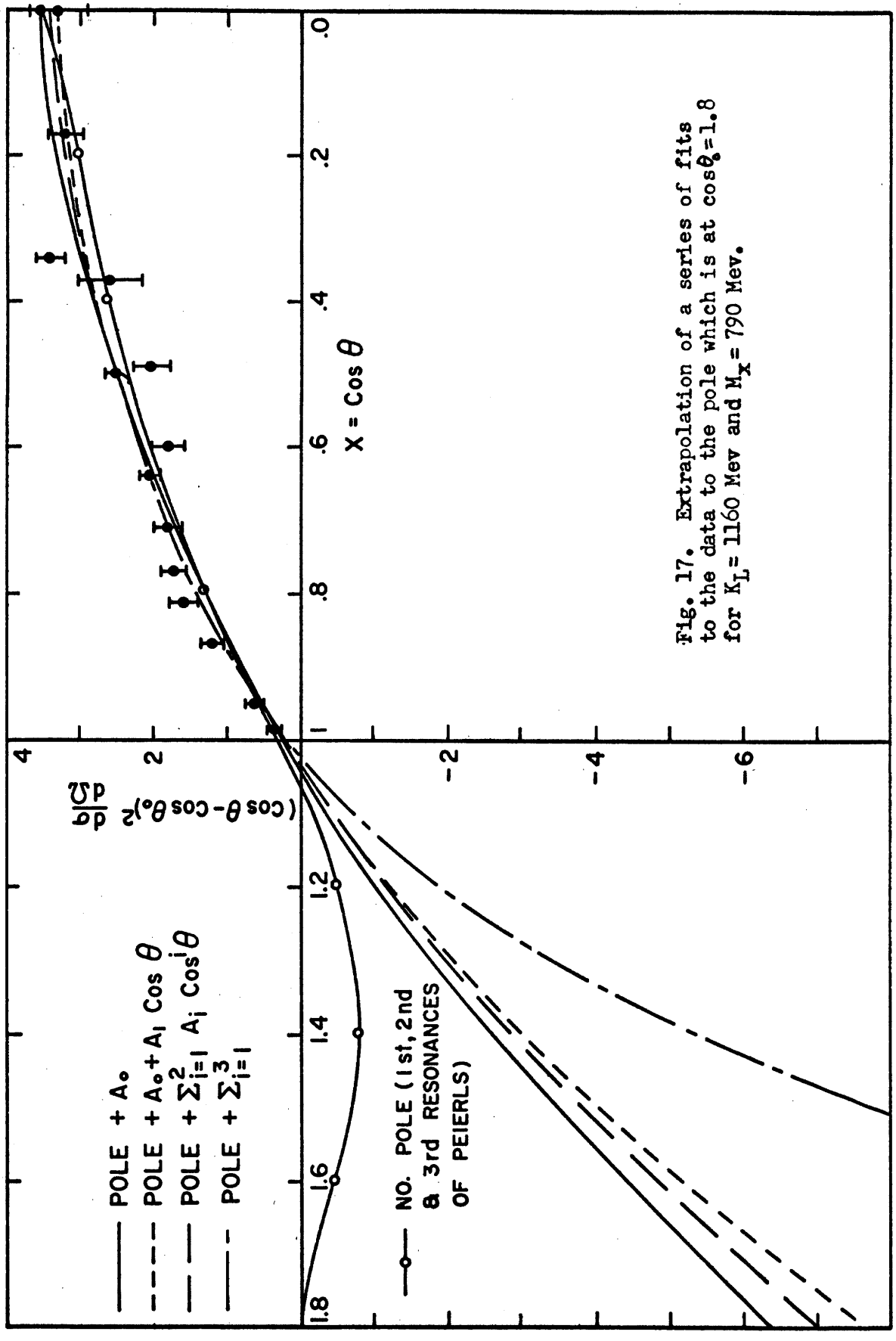

Fig. 17. Extrapolation of a series of fits to the data to the pole which is at $\cos\theta_0 = 1.8$ for $K_L = 1160$ Mev and $M_X = 790$ Mev.

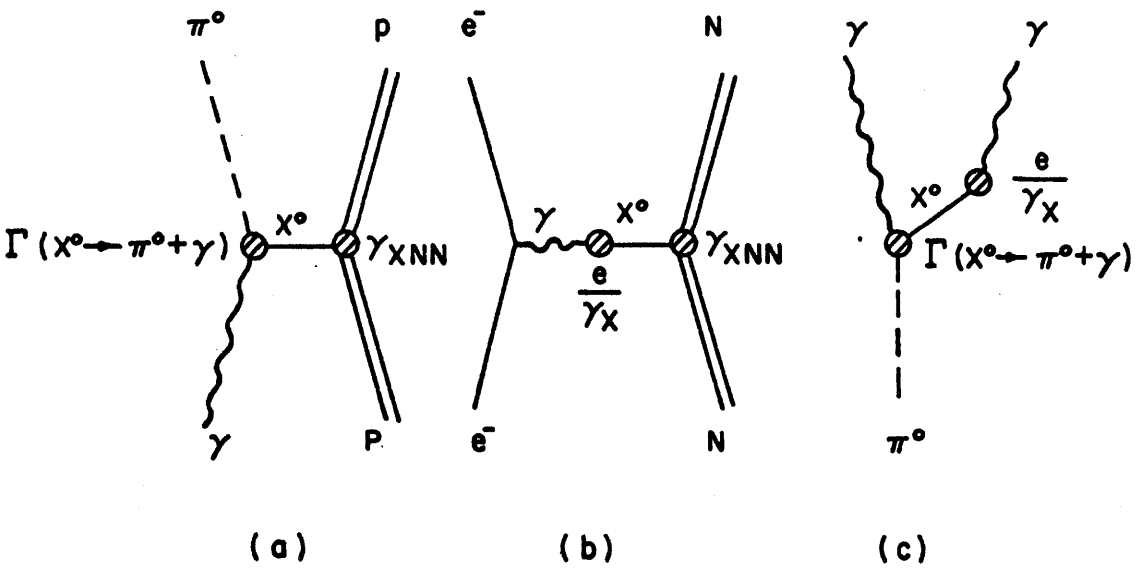

Fig. 18. Feynman diagrams for some simple processes containing the coupling constants γ_X, γ_{XNN} and $\Gamma(X^\circ \to \pi^\circ + \gamma)$

$\gamma + p \rightarrow p + \pi^0$

at selected energies using as few as four multipoles of which three are those suggested by Peierls (20) as being responsible for the 1st, 2nd, and 3rd resonances and are constrained to have "reasonable" phases and one (e.g. s-wave) is empirically added. At present it is difficult to say whether such fits are in any way unique or significant. Such a fit is shown in Fig. 17. Also recent pion scattering experiments at these energies described by Moyer (21), which are considerably more precise than photoproduction data, cannot be obviously understood in terms of single resonant states. Nevertheless, our data can no doubt be fit without any vector meson exchange poles.

With these reservations let us consider some consequences of our best estimate of the constant $\Gamma(\omega^0 \rightarrow \pi^0 + \gamma)(\gamma_{\omega NN}^2/4\pi)$ which is 0.5 Mev. Gell-Mann and Zachariasen (22) have given a prescription for calculating $\Gamma(\omega^0 \rightarrow \pi^0 + \gamma)$ and $\gamma_{\omega NN}$ individually as well as another coupling constant γ_ω which they define. This possibility requires knowledge of the π^0 lifetime, one of the isoscalar form factors and $\Gamma(\omega^0 \rightarrow \pi^0 + \gamma)(\gamma_{\omega NN}^2/4\pi)$ and is illustrated in Fig. 18 . Fig. 18 (a) implies our equation (4) while Figs. 18 (b) and 18 (c) imply equation 4.22 of reference (22)

$$F_1^S(s) \approx \left(\frac{\gamma_{\omega NN}}{\gamma_\omega}\right)\left(\frac{-M_\omega^2}{s - M_\omega^2}\right) + \left(1 - \frac{\gamma_{\omega NN}}{\gamma_\omega}\right) \qquad (5)$$

where $F_1^S(s)$ is the Dirac isoscalar form factor.

and equation 5.12* of reference (22).

$$\frac{\Gamma(\omega^o \to \pi^o + \gamma)}{\Gamma(\pi^o \to \gamma + \gamma)} = 2\left(\frac{M_\omega^2 - \mu^2}{M_\omega \mu}\right)^3 \left(\frac{\gamma_\omega}{\ell}\right)^2 \qquad (6)$$

Taking $\gamma_{\omega NN}/\gamma_\omega = 1{\cdot}2$ (23) and the π^o lifetime as 1.9×10^{-16} sec and solving the three equations we get

$\Gamma(\omega^o \to \pi^o + \gamma) = 240$ Kev, $(\gamma_{\omega NN}^2/4\pi) = 2.0$ and

$(\gamma_\omega^2/4\pi) \simeq 1.7$.

In conclusion let us consider some experimental investigations which are motivated by these results. First of all more careful π^o photoproduction measurements are necessary. It should be possible to obtain, say 5%, measurements at closely spaced angles and fixed energy, say 1.3 Bev, over the whole angular region. If our interpretation is correct that a vector meson pole is beginning to dominate the cross section above the third resonance then the extrapolation to the pole could be carried out with confidence even though the pole is a long way from the physical region. For this particular investigation it is most unfortunate that previous investigators have confined their measurements to C.M. angles of 60^o, 90^o, and 120^o.

Our 0^o measurements are surprising and interesting even in the absence of any interpretation since one might not expect the cross section at 0^o to be small at all energies. It is interesting to note that since the cross section for

$$\gamma + p \to p + \pi^o \qquad (7)$$

---

* This equation has been changed by a factor of 4 by which it was incorrect in the original.

is small in the forward direction it becomes easier to measure

$$\gamma + n \rightarrow n + \pi^0 \tag{8}$$

in the forward direction indirectly by measuring

$$\gamma + d \rightarrow d + \pi^0 \tag{9}$$

It would be interesting to see if the cross section for (8) is small at 0° as is suggested by the 1st order Born approximation. Process (9) is also useful in principle and perhaps in practice for isolating the separate contributions of ω^0 and ρ^0 poles.

Another interesting piece of information which might be soon forthcoming is a direct measurement of $\Gamma(\omega^0 \rightarrow \pi^0 + \gamma)$ which we estimate to be 240 Kev. This could perhaps be measured by a direct measurement of $\Gamma(\omega^0 \rightarrow$ anything) which is known to be $\lesssim$ 10 Mev (25) and a measurement of the branching ratio $\Gamma(\omega^0 \rightarrow \pi^0 + \gamma) \div \Gamma(\omega^0 \rightarrow$ anything). It is known that $\Gamma(\omega^0 \rightarrow$ neutrals$) \div \Gamma(\omega^0 \rightarrow \pi^0 + \pi^+ + \pi^-) \approx 14\%$ (26). If we assume that the dominant neutral mode is $\omega^0 \rightarrow \pi^0 + \gamma$ and the dominant overall mode is $\omega^0 \rightarrow \pi^0 + \pi^+ + \pi^-$ then our estimate $\Gamma(\omega^0 \rightarrow \pi^0 + \gamma) =$ 240 Kev leads to an estimate $\Gamma(\omega^0 \rightarrow$ anything$) = 1.7$ Mev.

APPENDIX A. EQUIPMENT

a) The Synchrotron Beam

The Caltech synchrotron accelerates about 2×10^9 electrons to an energy of E_o once per second. When the electrons are at full energy the synchrotron magnetic field is held constant, while the accelerating field is set to be too low to make up for the radiation energy losses of the circulating electrons. As a result the electrons spiral into a 0.2 radiation length thick tantalum target, in a slow and controllable way, over a time of about 60 msec. The resultant bremsstrahlung beam of photons is collimated primarily by a 12" thick collimator with a 1/4"x3/8" hole about 7 ft. from the radiator. The beam then passed in order through a thin walled air ionization chamber, a lead scraper, the H_2 target of this experiment (and part of the time a surrounding magnet of this experiment), another lead scraper, perhaps through targets for other experiments and then into a beam catching ionization chamber.

When beam monitoring was done using the beam catching chamber it was necessary to correct for losses of beam in targets downstream from ours. The loss of beam at the scrapers was negligible. A possible source of concern was the electron content of the beam, (originating, presumably, in the collimator). This could have caused faulty beam monitoring as well as electron initiated backgrounds. That the former effect was negligible was shown by comparing the beam intensity upstream and downstream with the sweeping magnetic field on and off. The latter effect was also negligible

as is shown in Appendix B (d).

It is well known that up to its end point energy E_0 the bremsstrahlung spectrum is given by

$$n(k)\,dk = Q\,\frac{B(\hat{k})}{\hat{k}}\,dk \qquad (10)$$

where Q(number of equivalent quanta) = W/E_0, W = the total energy in the beam and $B(\hat{K})$ is a factor close to 1. $B(\hat{K})$ has been measured by Boyden (27) who has also investigated the extent to which formula (10) is correct, e.g. he finds that $B(\hat{K})$ does not depend on E_0 except through $\hat{K}$.

Let us briefly describe the measurement of W and E_0. E_0 was measured by a beam energy meter which measured the magnetic field in the synchrotron during the beam dump. We call this value of E_0 the nominal beam energy. The counter configuration of this experiment also determined an absolute energy calibration, which we call E_0(counters), as will be explained in Appendix B (e). Owing to errors of unknown origin these disagreed by 2%.

$$E_0(\text{counters}) = E_0(\text{nominal}) \times \left[1 + 0.02 \pm 0.01\right] .$$

This uncertainty is most unfortunate since the upper end of the energy bite of this experiment was determined by the beam energy and the lower end by the counters. Accordingly we have used the beam calibration given by the counters

$$E_0 = E_0(\text{counters}).$$

In this way we hope to have minimized the error from this source.

The primary standard for measurement of W was a Wilson

quantameter with a response of $(5.0 \pm 0.2) \times 10^8$ Mev/Coulomb at S.T.P. The essential features of this quantameter are that its response is calculable and that its output for an incident photon is proportional to the energy of that photon. (In other words, the chamber calibration in Mev/Coulomb is independent of beam energy). R. Gomez (11) has checked both of these features at the Stanford linear electron accelerator and has found satisfactory agreement to within a few per cent.

During most of the running, secondary standards were used for beam monitoring. These were either the thin-walled air chamber just at the exit of the synchrotron or a thick-walled beam catcher. They were appropriately calibrated at each E_o.

Charge from the various monitors was measured in units of beam integrator pulses (called BIPS with 1 BIP = 0.2106 ± 0.0003 μCoul). A typical synchrotron beam intensity was 8 seconds per BIP with very large fluctuations. A typical π° counting rate was 1 count per 10 BIPS (or 1 count per minute).

b) Target

The liquid hydrogen target was a pressure fed target using a commercial 10 litre liquid nitrogen cooled dewar as a reservoir. The filling was controlled by two automatic valves (one on the helium gas pressurizing line, the other on the target exhaust) which reacted to a temperature sensing resistor placed in the target and above the beam line, in such a way as to keep the target full. This type of target was initially described by Littauer (28). Wilson (29) described a target like Littauer's except for having vacuum insulation and heat shields cooled by recirculating the evaporated hydrogen. Our target had these properties.

The active target volume was a cylinder 16.5 cm long and 4.8 cm in diameter. Owing to boiling in the feed line between the reservoir and the target cylinder there was a continuous procession of small bubbles passing up through the target cylinder and the beam, but this effect was small enough to be neglected.

c) γ-ray Counters

The two γ-ray counters were designed and built by R. Gomez, H. Ruderman and A.V. Tollestrup and are completely described in the laboratory report, C.T. S.L.-31. Any success which this experiment has achieved is due, in a large degree, to the desirable properties of these counters, and to the realization before the author became associated with the equipment, that they would be ideal for detecting π^0's in the high flux of particles in the forward direction from a bremsstrahlung beam.

In Appendix F various tests of the counters are described. Here we will just list some of the important or interesting properties of the two identical counters.

1) They are 14"x14"x12" lead glass "cubes" (density = 3.88 gm/cm^3, radiation length = 2.5 cm) which are viewed by nine R.C.A. type 7046, 5" phototubes.
2) They are remarkably insensitive to particles other than electrons and photons; protons essentially do not count while π's and μ's give pulses no higher than a 250 Mev photon or electron would give.
3) The charge output from the counters is proportional to the incident photon (or electron) energy at least from 200 Mev to 1 Bev. See Appendix F (i) and Fig. 25.

4) The counter resolution (or rather lack of resolution) is apparently due almost entirely to statistical fluctuations in the number of photo-electrons. See Appendix F (ii) and Fig. 26. Since the number of photo-electrons is proportional to the incident particle energy, and the width from statistical fluctuations is proportional to the square root of the number of photo-electrons we expect (and observe) the width to vary as the square root of the incident particle energy. (At 1 Bev the standard deviation is 80 Mev).

5) The counters are rather sensitive to stray magnetic fields with the gain changing by a few per cent for a field of a few Gauss. This made the maintenance of an absolute energy calibration rather difficult since, for example, the stray field of the synchrotron caused the counter gain during beam dump to depend slightly on the beam energy.

6) The pulse output of the counters is rather low. Hence the pulse from a 100 Mev photon had to pass through two Hewlett Packard distributed amplifiers to give a pulse of a few volts (big enough to operate a fast coincidence circuit). Consistent with this low signal output, was the rather low signal to noise ratio. The base-line wandering due to noise was equivalent to about $\pm$10 Mev.

d) Electronics

The electronics in this experiment was almost completely unchanged from that which Ruderman et al. used to detect π^0 photoproduced from complex nuclei near zero degrees. This electronics has been well described by H. Ruderman in his thesis and we do not repeat this. For reference, we have copied Figs. (19) and (20) which are block diagrams of the fast and slow electronics from H. Ruderman's thesis with the necessary slight modifications.

The only important change was that we used a dot plotter (Moseley X-Y plotter #35) for correlating the Cerenkov counter pulse heights (Ruderman took pictures of an oscilloscope). This proved to be quite convenient since as many as 100 events could be recorded on a single sheet of graph paper where they could be ticked off by hand in various sorting procedures. Partly as a result of the ease of this operation it was never necessary to digitize individual events and no data handling was performed with automatic computers. To achieve this end it was also convenient to keep the individual counter gains constant (usually at 80 Mev per 1/2 inch on the graph paper).

e) Physical Layout

In Fig. 4 is shown a view of the layout of the apparatus in relation to the rest of the synchrotron experimental area.

Fig. 19 BLOCK DIAGRAM OF FAST ELECTRONICS. For some runs there were slight differences. Coincidence between A and B is denoted by A.B. Also 1A or CR.B means either 1A or CR in coincidence with B.

All circuits are transistorized except for the distributed amplifiers. The figures in parentheses are the circuit drawing numbers. A brief description of the circuits follows.

MIXER: Adds nine input signals three at a time and then sums the triplets. Outputs for (123), (456), and (789) sums in addition to the 1-9 sum. Calibration input to the nine channels in parallel.

ATTN: Step attenuators.

HPA, HPB: Hewlett-Packard distributed amplifiers type 460A and 460B.

DELAY MIXER: Adding circuit with delay in each channel adjusted by external cables.

MULTI: Multiplexor with three emitter follower outputs for each input. (10-T-538)

F.C.: Fast coincidence circuit model 705. (10-T-468)

DOUBLE GATE AND ADDER: A pair of linear fast gates. The sum (A+B)g of the two gated signals is also available at the output. (10-T-618)

AMP: Slow, fixed gain amplifier Model 721. (10-T-549)

STCH: Linear stretching circuit to lengthen pulses to 0.25 μsec. The voltage of the flat-topped output pulse is proportional to the charge of the input pulse. There is a calibration input on each stretcher.

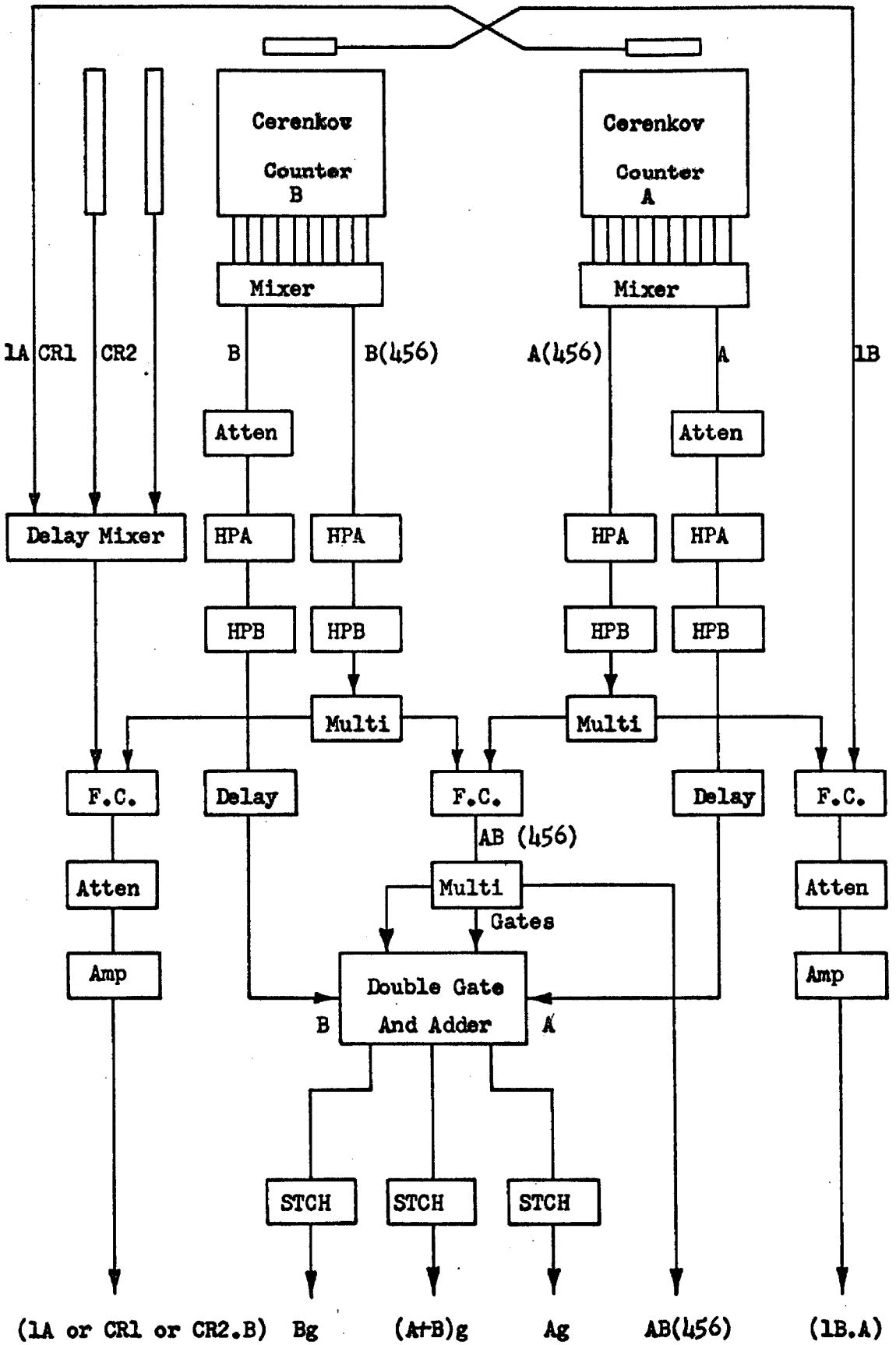

FAST ELECTRONICS BLOCK DIAGRAM

Fig. 20. BLOCK DIAGRAM OF SLOW ELECTRONICS. For some runs there were slight differences from what is shown. When protons were being detected there were fairly large changes. In particular, it was necessary to sacrifice the veto counters 1A and 1B to free electronics for the proton counter.

$\overline{1B.A}$ means that the signal 1B.A is required to be not present. A brief description of the circuits follows.

522A: 0.1 μsec rise time, 0-2.5x10^3 gain amplifier.

KECK BOX: Two three channel coincidence-anti-coincidence circuits (123) and (456) followed by a coincidence between the outputs of the first two (123456).

SCAL: Decimal scaling unit.

KICKSORTER: Twenty channel pulse height analyser.

GATED STRETCHER: Amplitude preserving pulse stretcher.

X-Y PLOTTER: Moseley Model 35 plotter rewired to respond to D.C. voltages on its 2 inputs by placing a dot on a sheet of graph paper at the appropriate place.

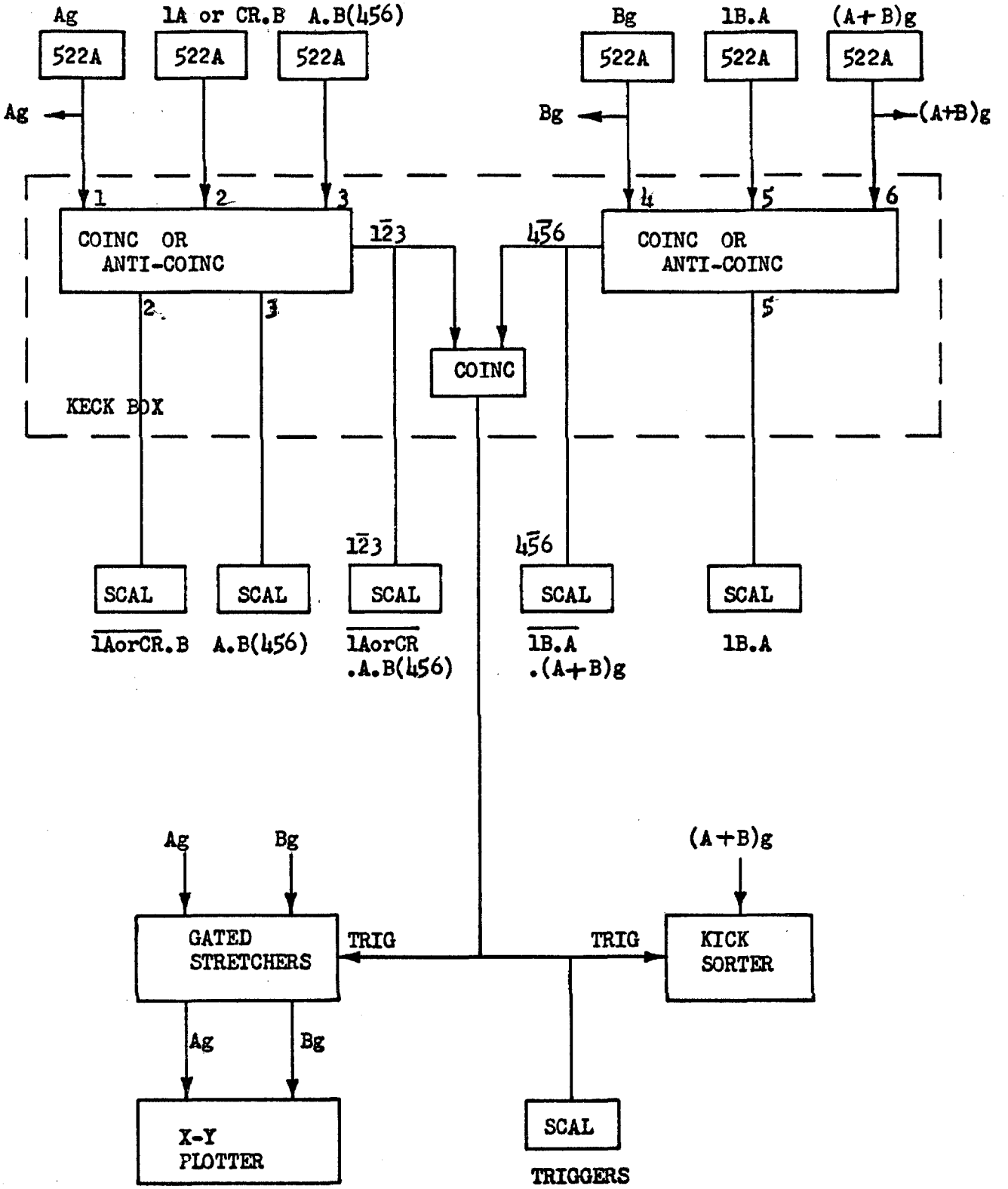

SLOW ELECTRONICS BLOCK DIAGRAM

APPENDIX B EXPERIMENTAL DETAILS

a) Calibration

An individual counter gain, if left to itself, drifted around by about±5% from week to week. It was possible to correct for this, and leave a gain error ± 2%, by observing the position of the peak in the counter from the passage of cosmic rays over a period of about 10 minutes per counter. These were presumably mainly minimum ionizing μ mesons. The position of this peak was used as a secondary gain standard and the gains were reset evert day or two. The primary calibration was done using a mono-energetic electron beam of known energy which is described in Appendix F. At that time the positions of the cosmic ray peaks were found to correspond to 220 Mev photons in counter A and 235 Mev in counter B.

b) Aperture Definition

The apertures were defined as holes (usually 8" across and 6" high) in 8" thick lead walls. For most of the runs these apertures were backed by scintillators which vetoed photons converting in the sides of the hole. This configuration presumably defined the apertures very well to be just negligibly larger than the physical size of the hole seen from the target.

When the recoil proton was being detected these aperture-backing counters were sacrificed for want of electronics to handle the signals. This had three undesirable, although not serious, effects. First, the aperture became somewhat poorly defined since photons hitting the sides of the hole might or might not count. To minimize this effect the apertures were shaped so that the sides pointed approximately toward the target. This effect led to a 5% systematic error

for the "with proton" data. Second, the measured photon energy spectra were distorted by the loss of energy of those photons which hit the edges but were still counted. This effect is evidently correlated with the first since if too much energy was lost in the wall an event would have been discarded on the basis of too low pulse height. To this extent, pulse height in the counters helped to define the aperture. Third, a background of true events giving particles from the target, one or both of which was charged, became possible. This background was found to be negligible at the one point where it was measured.

c) Accidentals and fast counting rates

Undoubtedly the most likely causes for serious error against which we had to guard in this experiment resulted from the high flux of particles near the forward direction where the measurements were made. Forward of about 10° in the laboratory it was necessary to place the target inside a magnetic field to sweep away pair produced electrons and other charged particles. Nevertheless the rates were very high. The difficulties caused by these high rates fell into three categories: flooding of the electronics, accidental coincidences, and accidental vetoing (or dead-time).

i) Flooding of the electronics. Most electronics will malfunction if confronted with too high counting rates. Likely results are: lowered phototube gains, lowered coincidence circuit output pulses, lowered amplifier gains and miscounting by scalers. These effects were investigated and found to be not serious. The output spectra of all the coincidence circuits (for events with reasonably large Cerenkov counter pulse heights) were well-peaked with only a small lower tail, presumeably due to accidentals.

An operational test of the electronics was the following. A small counter (LIT) was placed in front of scintillator 1A (which was in front of Cerenkov counter A). In this configuration LIT.A coincidences should always have been accompanied by 1A pulses, or equivalently the LIT.A.$\overline{1A}$ rate should be zero. This rate was found to be 3% of the LIT.A rate. This small discrepancy (which was not at all serious) could have been the result of malfunctioning, of A.1A accidentals, or of showers which counted in LIT and in A but skipped 1A. The situation is summarized by saying that 1A had an efficiency of at least 97%. The success of this test indicated that much of the electronics was not being seriously flooded. Another operational test was made possible by the Cerenkov counter $K_1 + K_2$ energy spectrum during actual runs as shown in Fig. 7. The existence of distinct π^o peaks implied that serious flooding was not taking place. The fact that the measured spectra agreed rather well with the expected spectra implies that the counter gains were not sagging. At 5° and larger angles in the laboratory this check was available but inside this the π^o peak disappeared because the cross section became so small.

ii) Accidental Coincidences. It was possible for A and B to be in accidental coincidence and simulate a π^o event. That this was not serious is evident from the $K_1 + K_2$ spectra, Fig. 7. Accidental coincidences would preferentially give low $K_1 + K_2$ pulses. Some such low pulses from accidentals were present but they merely enhanced the low energy background which was already present.

iii) Accidental Vetoing. As explained, effects (i) and (ii) could be ignored with high confidence purely on the basis of the clean π^o peak in the $K_1 + K_2$ spectrum. The effect we now discuss was

much more elusive and dangerous. Dead time in the Keck box (slow coincidence anti-coincidence circuit) was only about 0.1% at worst, but dead time due to the fast rates in the veto counters was serious. Some fraction of all B pulses were accidentally in coincidence with 1A pulses. This same fraction of all π^0 events evidently were accompanied by 1A.B pulses and hence were rejected. The overall vetoing fraction $\underline{a}$ was as high as 25% for some runs but almost all runs with $\underline{a}$ over 15% were discarded. To make the necessary corrections to the data $\underline{a}$ had to be measured at each point. This, of course, was difficult and the error in $\underline{a}$ was assigned to be 100%. i.e. if C.R. stands for counting rate

$$\text{C.R.(measured)} = \text{C.R.(true)} \times (1 + \underline{a} \pm \underline{a}). \qquad (11)$$

In two cases this error assignment was larger than the statistical counting error but for most points it was almost negligible. Each veto counter contributed to this effect but the cosmic ray counters were the worst offenders. To measure $\underline{a}$ for a single counter, say 1B, the rate 1B.A which was essentially all accidentals was monitored continuously and the rate A.A was measured using the 1B.A coincidence circuit with 1B replaced by A (A.A counts were proportional to the amount of beam and hence could be measured just once, while 1B.A counts depended on the beam intensity and had to be monitored). We then had

$$a = \frac{C.R.(1B \cdot A)}{C.R.(A \cdot A)}$$

If the pulses in question had had uniform pulse heights this prescription would have been rigorous. Since they did not, non-ideal behaviour

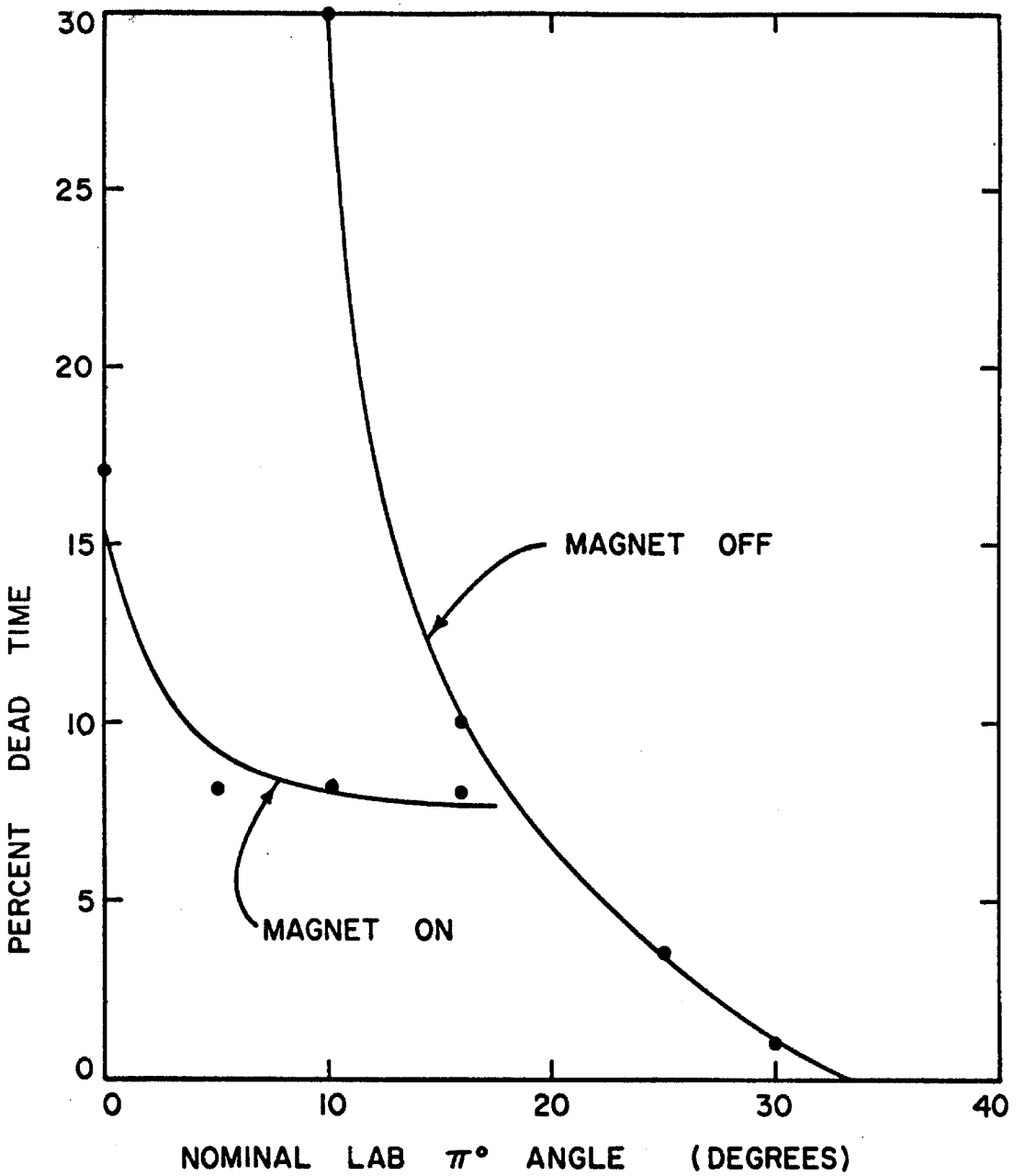

Fig. 21. Curves showing percentage dead time due to high counting rates in veto counters both with the sweeping magnet on and off for the series of data with $\bar{K}$ near 1150 Mev.

of the fast coincidence circuit could have distorted the measurement and we have accordingly assigned a large error. For our K=1150 data the value of a as a function of angle with the magnet on and off is shown in Fig. 21.

d) Backgrounds

There were several processes which could give two coincident γ -rays. Most such processes, however, would preferentially have given low $K_1 + K_2$ signals. But we observed fairly clean π° peaks in the $K_1 + K_2$ spectra (see Fig. 7) and hence such processes could not have been serious.

One annoying background which fell into this low energy category consisted of individual cosmic ray particles which passed through both counters. These necessitated the use of large anti-coincidence counters between the two Cerenkov counters. These counters at forward angles were very near the beam and accordingly counted very fast, which aggravated the accidental vetoing problem.

The chief effect of these "low energy backgrounds" was to introduce a systematic error coming from incorrect division of events into π° events and low energy events. The situation is shown in Fig. 7 which shows $K_1 + K_2$ histograms for the angular distribution at an average incident lab photon energy near 915 Mev. The slant line in Fig. 7 shows the empirically chosen bias. All events falling below this bias were discarded while all above it were called π°'s.

A more dangerous background was π°'s coming from a process other than single π° photoproduction. e.g.

$$\gamma + p \rightarrow p + \pi^\circ + \pi^\circ \qquad \pi^\circ \rightarrow \gamma + \gamma \qquad (12)$$

or

$$\gamma + p \rightarrow n + \pi^+ + \pi^0 \qquad (13)$$
$$\pi^0 \rightarrow \gamma + \gamma$$

The $K_1 + K_2$ spectrum for π^0's from this process is evidently quite similar to the spectrum from singly-produced π^0's. At a fixed angle and with a fixed beam energy there was a maximum energy E_{max} (1π) for a singly-produced π^0's and a lower maximum energy E_{max} (2π) for a π^0 from a π-pair. Also the counters determine a minimum energy E_{min} (counters) of any π^0 which could be detected. Ideally one would adjust things so that

$$E_{max}\ (2\pi) < E_{min}\ (\text{counters}) < E_{max}\ (1\pi)$$

in order to exclude all but singly-produced π^0's. This was unfortunately impossible because the integrated effective solid angle

$$\int_{E_{min}(\text{counters})}^{E_{max}(1\pi)} Y(E_\pi)\, dE_\pi$$

would have been too small with a resultant low counting rate. The typical situation is illustrated in Fig. 22 where

$$E_{min}\ (\text{counters}) = 950 \text{ Mev},$$
$$E_{max}\ (1\pi) = 1280 \text{ Mev},$$
$$E_{max}\ (2\pi) = 1120 \text{ Mev}.$$

Using this figure we can estimate the background from π-pairs. For this calculation we assume that the beam spectrum is constant up to its end point where it cuts off sharply. We ignore the difference between the C.M. system and the laboratory system and we assume that π-pairs are produced isotropically with the total cross section for processes (12) and (13) being 50 μbarns. This is approximately the total cross section measured by Cocconi et al. (30) for the process

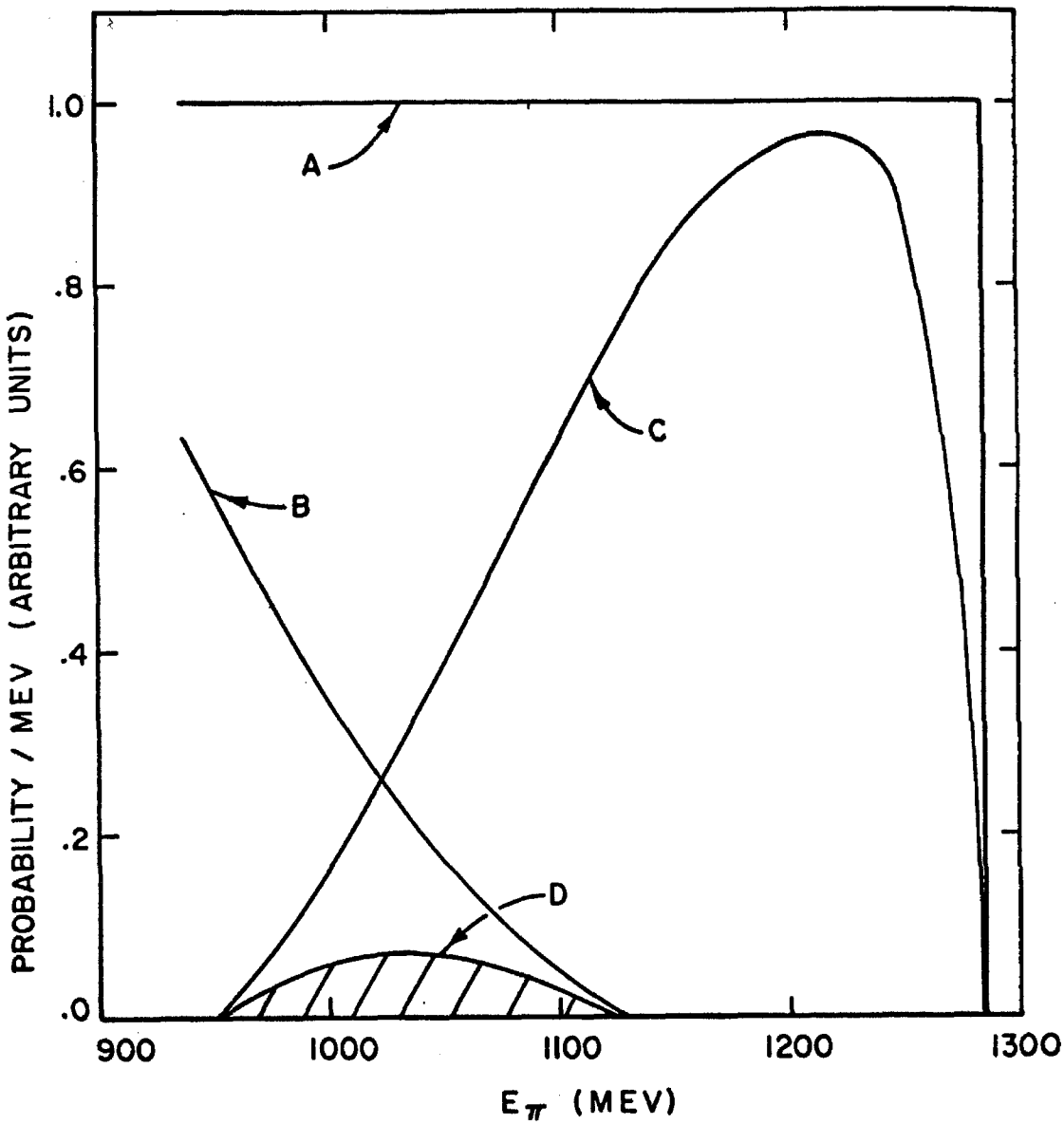

Fig. 22. Curves illustrating π-pair rejection under simplifying assumptions described in the text.
A: Spectrum of π^0's from single π^0 photoproduction for a constant total cross section of 10 μbarns.
B: Spectrum of π^0's from a π-pair photoproduction for a constant total cross section of 50 μbarns.
C: Detector resolution function.
D: B multiplied by C.
The background to foreground ratio is the area under D divided by the area under C. (approximately 5%).

$$\gamma + p \rightarrow p + \pi^+ + \pi^- \qquad (14)$$

We assume that the energy distribution of the individual π^0's from π -pairs is given entirely by phase space. One factor which discriminates against π -pairs is the scarcity of events in which a single π^0 gets enough energy to be counted. (See the energy distribution function, curve B. Fig. 22). Also the effective solid angle tends to be quite small for these π^0's. (See curve C. Fig. 22). The counting rate from π -pairs is obtained by integrating the energy distribution function multiplied by the effective solid angle. This integral is given graphically by the shaded area in Fig. 22. The single π^0 counting rate is proportional to the area under curve C. (for a total cross section of 10 μbarns, which is typical). With the assumptions we have made processes (12) and (13) were expected to simulate a C.M. differential cross section for single π^0 production of about 0.04 μ barn/ster. Since this estimate could easily be wrong by a factor of two or more we have made no correction for this source of error but merely note that the contamination is not too serious.

Empty target backgrounds were typically 10% when just the γ -rays were detected and 1% when the proton also was detected.

e) Consistency Checks

We will mention various consistency checks which hopefully would have shown up any serious blunders.

i) A π^0 photoproduction cross section from Carbon was measured and compared with a previous measurement (using the same equipment) of H. Ruderman. This gave agreement.

ii) At wide angles the sweeping magnet was not needed but on the other hand the π^o counting rate should not have depended on whether or not it was on. Although all the single-counter rates depended rather drastically on whether or not the magnet was on, the π^o rate did not.

iii) The energy spectra of detected photons agreed rather well with the expected spectra. In Fig. 6 is shown the expected and observed K_1+K_2 spectrum for a typical case. In Fig. 8 is shown the K_1-K_2 spectrum expected and observed for a typical case for those events with K_1+K_2 high enough to be from a π^o. The agreement was judged adequate.

iv) When measurements were taken at the same angle and photon energy but with different configurations (for example, with and without proton) the measurements agreed fairly well, although not within errors. See Fig. 12.

v) A resolution curve was run in which the counter configuration was held constant and the beam energy was varied. The result is shown in Fig. 9. The agreement between calculation and measurement can be made excellent by assuming an error in the beam energy calibration of 2% as explained in Appendix A (a).

APPENDIX C. RESULTS (TABLES)

TABLE NO. 1. EXCITATION CURVE (θ_{π}(C.M.) = 50°)

Point No.	End Point Energy (Mev) (nominal)	No. of Counts/10	Full Counting Rate/10^3 Bips	Empty/10^3 Bips	Empty Error	Counting Error %	Error from 1% Error in End Point %	Dead Time Error %	Total Error %	Pion Efficiency (C.R./10 Bip-/μbarn)	Proton Efficiency %	C.M. Pion Angle	K-Mean Incident Lab Energy (Mev)	C.M. Cross Section (μbarns/ster)	Error
1	850	13	85	13	6	14	1	2	14	.380	N/A	50	743	1.89	.26
2	900	26	66	10	5	9	2	3	10	.440		50	800	1.27	.13
3	950	9	68	4	4	15	3	3	16	.485		50	853	1.20	.19
4	1000	24	75	10	3	9	4	3	10	.522		50	907	1.26	.13
5	1050	36	91	9	3	7	5	3	10	.547		50	957	1.47	.15
6	1100	36	119	8	4	7	6	4	10	.560		50	1007	1.98	.20
7	1150	26	103	7	3	8	6	4	11	.575		50	1058	1.65	.18
8	1200	33	99	6	2	7	7	4	11	.557		50	1108	1.66	.18
9	1250	13	100	5	3	10	8	5	14	.596		50	1153	1.59	.22
10	1300	9	79	4	4	11	9	5	15	.548		50	1206	1.37	.21

TABLE NO. 2. ANGULAR DISTRIBUTION ($\bar{K}$ Near 750 Mev, E_o = 875 Mev)

Point No.	Lab Pion Angle (nominal)	No. of Counts/10	Full Counting Rate/10^3 Bips	Empty/10^3 Bips	Empty Error	Counting Error %	Error from 1% Error in End Point 1%	Dead Time Error %	Total Error %	Pion Efficiency (C.R./10 Bip-μbarn)	Proton Efficiency %	C.M. Pion Angle	$\bar{K}$-Mean Incident Lab Energy (Mev)	C.M. Cross Section (μbarns/ster)	Error
11	0	3	46	16	13	53	6	20	57	.738	N/A	3	784	.42	.24
12	5	8	69	17	11	28	4	16	32	.769		9	771	.67	.19
13	10	8	87	20	8	20	2	15	25	.739		16	759	.91	.23
14	16	7	89	20	6	18	2	10	21	.642		26	750	1.07	.22
15	20	7	74	18	7	20	1	8	22	.557		32	744	1.02	.22
16	25	10	88	16	8	16	1	4	17	.471		39	741	1.52	.26
17	30	6	78	13	9	21	1	2	21	.376		47	741	1.73	.36

TABLE NO. 3. ANGULAR DISTRIBUTION ($\bar{K}$ Near 915 Mev, E = 1020 Mev)

Point No.	Lab Pion Angle (nominal)	No. of Counts/10	Full Counting Rate/10^3 Bips	Empty/10^3 Bips	Empty Error	Counting Error %	Error from 1% Error in End Point %	Dead Time Error %	Total Error %	Pion Efficiency (C.R./10 Bip-/μbarn)	Proton Efficiency %	C.M. Pion Angle	$\bar{K}$-Mean Incident Lab Energy (Mev)	C.M. Cross Section (μbarns/ster)	Error
18	0	8	31	8	4	21	8	27	35	.858	N/A	3	929	.27	.09
19	5	5	46	8	4	20	8	9	23	.841		10	928	.45	.10
20	10	8	80	8	4	14	7	5	17	.808		17	927	.89	.15
21	16	19	104	8	4	8	7	15	18	.721		27	922	1.33	.24
22	20	17	103	8	4	8	6	5	11	.644		33	922	1.47	.16
23	25	24	77	8	4	9	5	4	11	.565		41	916	1.22	.13
24	30	27	70	8	4	8	4	2	9	.484		49	909	1.28	.11
25	35	15	51	8	4	12	3	2	13	.399		56	899	1.07	.14

TABLE NO. 4. ANGULAR DISTRIBUTION ($\bar{K}$ Near 1150 Mev, E = 1280 Mev)

Point No.	Lab Pion Angle (nominal)	No. of Counts/10	Full Counting Rate/10^3 Bips	Empty/10^3 Bips	Empty Error	Counting Error %	Error from 1% Error in End Point %	Dead Time Error %	Total Error %	Pion Efficiency (C.R./10 Bip-μbarn)	Proton Efficiency %	C.M. Pion Angle	$\bar{K}$-Mean Incident Lab Energy (Mev)	C.M. Cross Section (μbarns/ster)	Error
26	0	4	17	6	3	33	2	16	37	.539	N/A	3	1097	.21	.08
27	5	8	37	8	4	16	2	8	18	.516		9	1101	.56	.10
28	10	13	94	10	4	11	4	8	14	1.020		18	1122	.82	.12
29	16	33	123	11	3	6	5	8	11	.787		29	1135	1.42	.16
30	20	30	111	10	4	7	6	6	11	.618		36	1151	1.64	.18
31	25	27	82	8	4	7	9	4	12	.489		45	1168	1.51	.18
32	30	21	54	5	2	8	9	2	12	.401		53	1167	1.22	.18
33	35	19	44	5	3	10	8	0	13	.332		61	1164	1.17	.15
34	40	7	41	5	4	15	7	0	17	.282		68	1158	1.28	.22

TABLE NO. 5. ANGULAR DISTRIBUTION ($\bar{K}$ Near 1170 Mev, E = 1330 Mev) PROTONS DETECTED

Point No.	Lab Pion Angle	No. of Counts/10	Full Counting Rate/10^3 Bips	Empty/10^3 Bips	Empty Error	Counting Error %	Error from 1% Error in End Point %	Dead Time Error %	Total Error %	Pion Efficiency (C.R./10 Bip-μbarn)	Proton Efficiency %	C.M. Pion Angle	$\bar{K}$-Mean Incident Lab Energy (Mev)	C.M. Cross Section (μbarns/ster)	Error
35	16	16	56	0	0	8	6	0	10	.974	.43	30	1185	1.32	.13
36	22	65	86	0	0	4	6	0	8	.882	.62	40	1180	1.59	.13
37	28	73	85	0	0	4	5	0	6	.738	.77	50	1179	1.52	.09
38	34	47	74	0	0	5	5	0	7	.637	.78	60	1171	1.48	.10
39	41	60	70	0	0	4	4	0	6	.524	.85	70	1162	1.57	.09
40	48	26	43	0	0	6	3	0	7	.398	.89	80	1159	1.22	.09
41	56	11	21	0	0	10	4	0	11	.258	.90	90	1170	.90	.10
42	65	9	11	0	0	11	4	0	12	.151	.90	100	1180	.83	.10

APPENDIX D. EVALUATION OF THE EFFECTIVE SOLID ANGLE

(a) Approximate Analytic Method

As described in Section II, the important quantity for calculating cross sections from counting rates is $Y(E_\pi)$, the effective solid angle. For finite counters this involves integration over the two counters and over π° directions which we shall now do.

Consider first two small counters of solid angles $d\Omega_1$ and $d\Omega_2$ on a unit sphere which has an isotropic point source of π°'s of energy E_π at its center P. See Fig. 23.

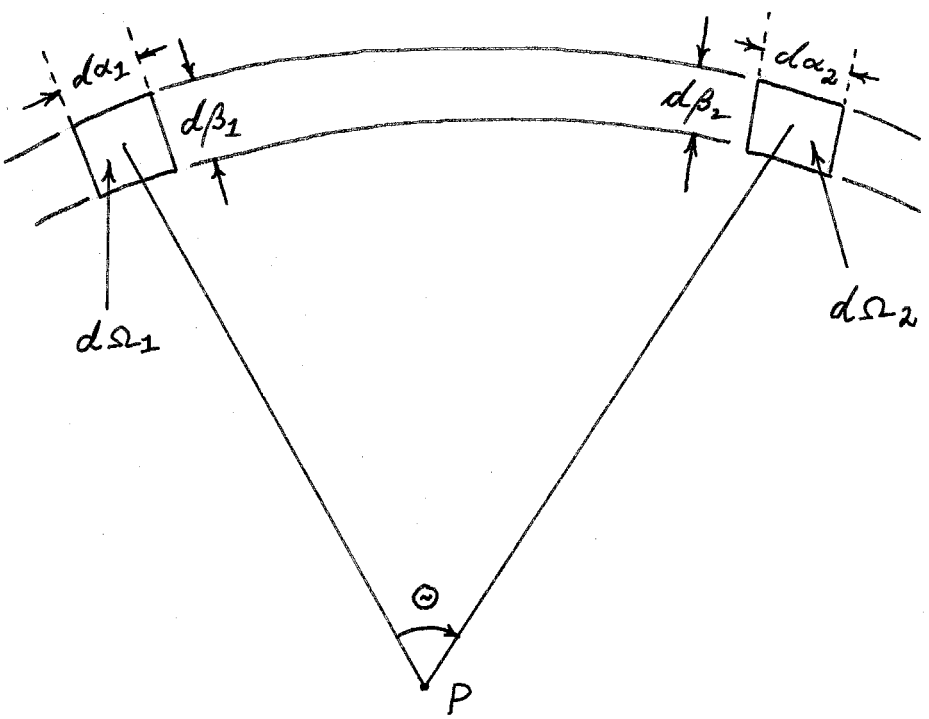

Fig. 23.

We wish to know the effective solid angle $dY(E_\pi)$ of the two counters for detecting π°'s of energy E_π. $dY(E_\pi)$ is given by an integral over the possible π° directions, $\vec{n}$, weighted by the detection probability $d\eta(E_\pi, \vec{n})$ that a π° of energy E_π travelling in the direction

$\vec{n}$ will give one photon through $d\Omega_1$, and one through $d\Omega_2$. Hence

$$d\gamma(E_\pi) = \int_{\substack{\text{unit} \\ \text{sphere}}} d\Omega \, d\eta(E_\pi, \vec{n}). \tag{15}$$

$d\eta(E_\pi, \vec{n})$ is evidently non-vanishing only in a small region centered between the two counters. It is assumed that the distribution of π^0's is uniform over this region. Since $d\gamma(E_\pi)$ is a differential proportional to $d\Omega_1$ and $d\Omega_2$ we can write

$$d\gamma(E_\pi) = y(E_\pi)\, d\Omega_1 d\Omega_2 . \tag{16}$$

$y(E_\pi)$ is a function of the positions of the two counters.
But, again assuming that the π^0's are isotropic, $y(E_\pi)$ is a function only of the angle Θ between the two counters. Hence we write $y(E_\pi, \Theta)$, where now the only dependence on counter position has been made explicit. Our plan then, is to obtain

$$y(E_\pi, \Theta) d\Omega_1 d\Omega_2 = \int_{\substack{\text{unit} \\ \text{sphere}}} d\Omega \, d\eta(E_\pi, \vec{n}) \tag{17}$$

in preparation for integrating over actual finite counters C_1 and C_2 to obtain

$$\gamma(E_\pi) = \iint_{C_1 C_2} y(E_\pi, \Theta)\, d\Omega_1 d\Omega_2 \tag{18}$$

But $y(E_\pi, \Theta)\, d\Omega_1 d\Omega_2$ must equal 4π times the fraction of all π^0's of energy E_π emitted from P (and isotropic over the entire

unit sphere) which give one photon through each of $d\Omega_1$ and $d\Omega_2$. This, in turn, is some fraction of the fraction $\frac{2\,d\Omega_1}{4\pi}$ which give one photon into $d\Omega_1$. If $n(E_\pi, \omega)$ is the distribution in opening angle for π^0's of energy E_π then, looking again at Fig. 23 for definition of symbols, we find that of those π^0's which give a photon into $d\Omega_1$ a fraction

$$n(E_\pi, \omega)\, d\theta_2 \frac{d\beta_2}{2\pi \sin\omega}$$

also give a photon into $d\Omega_2$. An expression for $n(E_\pi, \Theta)$ is derived in Rossi (31) Equation (5) page 199 and is

$$n(E_\pi, \Theta) = \frac{m_\pi}{2p_\pi} \frac{\cos\Theta/2}{\sin^2\Theta/2 \sqrt{(E_\pi/m_\pi)^2 \sin^2\Theta/2 - 1}} \,. \qquad (19)$$

This expression diverges at the minimum opening angle which shows the great tendency of π^0's to decay with an angle near the minimum.

We can now gather our results, and get

$$y(E_\pi, \omega) = \frac{1}{4\pi} \frac{m_\pi}{p_\pi} \frac{1}{\sin^3\omega/2 \sqrt{(E_\pi/m_\pi)^2 \sin^2\omega/2 - 1}} \qquad (20)$$

Now for an actual counter configuration we must perform the integral indicated in (18). We can, however, exploit the fact that $y(E_\pi, \omega)$ depends only on ω (E_π being fixed throughout the entire calculation) and write

$$Y(E_\pi) = \int_{\text{Counters}} d\omega\, w(\omega)\, y(E_\pi, \omega) \qquad (21)$$

where, if L_{12} is the angle between the element $d\Omega_1$ and the element

$d\Omega_2$, then $w(\Theta)$ is given by

$$w(\Theta) = \iint_{\text{Counters}} d\Omega_1 d\Omega_2 \, \delta(L_{12} - \Theta). \tag{22}$$

$\delta(L_{12}-\Theta)$ here is a Dirac δ-function. $w(\Theta)$ is just the distribution in opening angles between pairs of points one in each counter.

So far we have proceeded exactly and, in fact, it is straightforward, for arbitrary counters, to evaluate $w(\Theta)$ and then $Y(E_\pi)$ using (21) and (22). For the configurations used during this experiment, however, certain fairly good approximations can be made which simplify things considerably. As a start, looking at Fig. 5 (a) in which counter dimensions are given as angles subtended at the target let us assume

$$\frac{\Delta\alpha}{\Theta_2} \ll 1. \tag{23}$$

In this approximation $w(\Theta)$ is evidently a triangular function

$$\begin{aligned} w(\Theta) &= (\Theta - \Theta_1)(\Delta\alpha)^2, && \Theta_1 < \Theta < \frac{\Theta_1+\Theta_2}{2} \\ &= (\Theta_2 - \Theta)(\Delta\alpha)^2, && \frac{\Theta_1+\Theta_2}{2} < \Theta < \Theta_2 \\ &= 0 && \text{elsewhere.} \end{aligned} \tag{24}$$

This approximation effectively shifts $w(\Theta)$ slightly toward smaller angles. This shift can be approximately compensated by using an effective Θ_2, $\Theta_2(\text{eff.})$ given by

$$\Theta_2(\text{eff.}) = \Theta_2\left(1 + \frac{1}{12}\left(\frac{\Delta\alpha}{\Theta_2}\right)^2\right)$$

and similarly for Θ_1. Typically Θ_2 is corrected here about +1%, which

is equivalent in its effect to a +1% change in beam energy.

Because of the double definition of $y(E_\pi, \Theta)$ in (20) it is convenient to define

$$Y(E_\pi, \bar{\Theta}) = \int_0^{\bar{\Theta}} = \int_{\Theta_{min}(E_\pi)}^{\bar{\Theta}} (\Delta\alpha)^2 (\bar{\Theta} - \Theta) y(E_\pi, \Theta)\, d\Theta \qquad (25)$$

where $\Theta_{min}(E_\pi)$ is given by

$$\left(\frac{E_\pi}{m_\pi}\right) \sin \frac{\Theta_{min}(E_\pi)}{2} = 1. \qquad (26)$$

$\Theta_{min}(E_\pi)$ is the minimum opening angle for a π^0 of energy E_π and is also the point at which $y(E_\pi, \Theta)$ diverges. Then $Y(E_\pi)$ is given by

$$Y(E_\pi) = Y(E_\pi, \Theta_2) - 2Y(E_\pi, \Theta_2 - \Delta\Theta) + Y(E_\pi, \Theta_1) \qquad (27)$$

where

$$Y(E_\pi, \bar{\Theta}) = (\Delta\alpha)^2 \int_{\Theta_{min}(E_\pi)}^{\bar{\Theta}} \frac{1}{4\pi} \frac{m_\pi}{p_\pi} \frac{(\bar{\Theta} - \Theta)\, d\Theta}{\sin^3 \Theta/2 \sqrt{(E_\pi/m_\pi)\sin^2 \frac{\Theta}{2} - 1}}. \qquad (28)$$

If we assume that

$$\frac{\Theta}{2} = \sin \frac{\Theta_2}{2} = \tan \frac{\Theta_2}{2} \qquad (29)$$

and similarly for all other pertinent angles since they are all smaller than Θ_2, we can perform this integral easily to get

$$Y(E_\pi, \bar{\Theta}) = A \frac{(\Delta\alpha)^2}{2\pi} \frac{1}{v_\pi^3} \left[a \cos^{-1} \frac{1}{a} - \sqrt{1 - \frac{1}{a^2}} \right] \qquad (30)$$

where v_π is the velocity of the π°,

$$a = \frac{E_\pi}{m_\pi} \sin \frac{\bar{\Theta}}{2}, \qquad (31)$$

and A is a term differing from 1 only in third order of small quantities. A is given by

$$A = 1 + \text{Order of} \left[\left(\frac{m_\pi}{E_\pi} \right)^2 (1 - a) \right]$$

The error in taking A = 1 was always less than 1%.

b) Monte Carlo Method

It is always straightforward although not always efficient to perform efficiency calculations for counter experiments using Monte Carlo methods and a high speed computer. The basic principle is that one can repeat the experiment in the computer as faithfully as desired. For this experiment such a computer program for the IBM 7090 has been written by C.R. Clinesmith. The basic sequence in this program is as follows

1) Randomly pick a photon from the correct beam spectrum and pick a target position.
2) Randomly pick a π° direction and calculate its energy and the proton direction in the reaction
   $\gamma + p \rightarrow p + \pi^\circ$
3) Randomly pick a π° decay and calculate the γ-ray directions.

4) Did the γ-rays hit the counters? If no, start over; if yes, continue.

5) Did the proton hit the proton counter? Tally accordingly and start over.

By tallying successes and failures one can obtain the required efficiencies except for statistical fluctuations.

APPENDIX E. EVALUATION OF THE POLE DIAGRAM

As mentioned in the Introduction we have largely followed Moravcsik (5) in attempting to isolate the vector meson pole process. He evaluates the pertinent matrix element in detail. Here we will merely sketch the results in order to clarify the quantities involved and make slight changes.

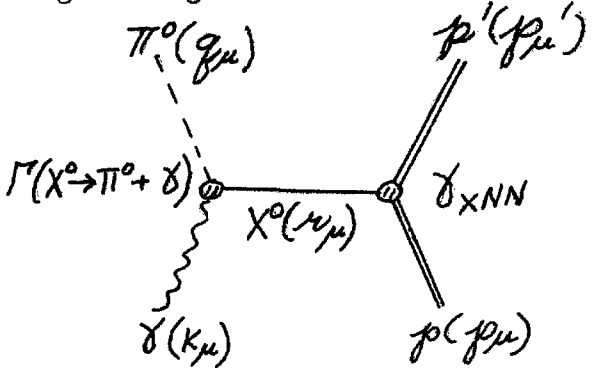

Fig. 24. Pole diagram. 4-momenta are given in parentheses.

First let us consider the γ, π^o, X^o vertex in Fig. 24 and assume that X^o is a vector meson. (The consequences are very much the same if X^o is a pseudo-vector meson and we refer the reader to reference (5) for a discussion of that case). If we assume that the form factor at this vertex is constant then we can write the coupling constant at this vertex in terms of the decay width $\Gamma(X^o \to \pi^o + \gamma)$. The simplest coupling at this vertex gives a matrix element

$$M = f_{X\pi\gamma}\, \epsilon_{\lambda\mu\nu\rho}\, K_\lambda\, \epsilon_\mu\, \eta_\nu\, \nu_\rho$$

$$\text{and} \quad f_{X\pi\gamma} = \left[\Gamma(X^o \to \pi^o + \gamma)\, \frac{96\pi \left(1 - \frac{\mu^2}{M_X^2}\right)^{-3}}{M_X^3} \right]^{\frac{1}{2}} \qquad (32)$$

where μ = mass of π^o.

M_X = mass of X^o.

$\epsilon_{\lambda\mu\nu\rho}$ = 0 if any sub-scripts are equal.

= 1 if $\lambda\mu\nu\rho$ is an even permutation of 1234.

$= -1$ if $\lambda\mu\nu\rho$ is an odd permutation of 1234.

K_λ = momentum 4-vector of the γ.

r_ρ = momentum 4-vector of the X^0.

ϵ_μ = polarization 4-vector of the γ.

η_ν = polarization 4-vector of the X^0.

At the X^0, p, p vertex the simplest coupling is

$$\sqrt{3}\,\gamma_{XNN}\,\bar{\psi}(p')\,\gamma_\mu\,\psi(p)\,\eta_\mu \tag{33}$$

where for ease in comparing with Gell-Mann and Zachariasen (22) the coupling constant has been chosen to be $\sqrt{3}\,\gamma_{XNN}$

$\bar{\psi}(p')$ = final proton spinor.

$\psi(p)$ = initial proton spinor.

γ_μ = conventional Dirac matrices.

η_μ = polarization 4-vector of X^0.

We can now follow the rules of Schweber (32) to compute the diagram of Fig. 24. Summing over polarizations of the intermediate vector meson one gets the matrix element to be ($\hbar = c = 1$),

$$T = C\,\frac{1}{r_\mu r_\mu - M_X^2}\,\epsilon_{\alpha\beta\gamma\delta}\,q_\alpha\,\epsilon_\beta\,K_\gamma\,\gamma_\delta \tag{34}$$

where the angular dependent factors are explicitly exhibited and where

$$C = -\frac{i}{(2\pi)^2}\,\frac{M_p}{2\sqrt{k\,q_0\,p_0\,p_0'}}\,f_{X\pi\gamma}\,\sqrt{3}\,\gamma_{XNN} \tag{35}$$

The 4-momenta of the photon, pion, X^0, incoming and outgoing protons are denoted by k_μ, q_μ, p_μ and p'_μ. We use the

convention $a_\mu b_\mu = a_o b_o - \vec{a}\cdot\vec{b} = a\cdot b$. M_p is the proton mass and ϵ_μ the photon polarization.

It is convenient to rewrite this matrix element in the form used by Chew, Goldberger, Low and Nambu (33), henceforth referred to as CGLN, who write a general π^0 photoproduction amplitude in terms of four fundamental forms.

$$\begin{aligned} M_A &= i\gamma_5 \not{\epsilon}\not{K} \\ M_B &= 2i\gamma_5 (P\cdot\epsilon\, q\cdot K - P\cdot K\, q\cdot\epsilon) \\ M_C &= \gamma_5 (\not{\epsilon}\, q\cdot K - \not{K}\, q\cdot\epsilon) \\ M_D &= 2\gamma_5 (\not{\epsilon}\, P\cdot K - \not{K}\, P\cdot\epsilon - i M_p \not{\epsilon}\not{K}) \end{aligned} \tag{36}$$

where $P = \frac{1}{2}(p+p')$. Manipulation of (34) yields the result that

$$T = C \frac{1}{\nu_\mu \nu_\mu - M_x^2} M_D . \tag{37}$$

For dealing with particular angular momentum states CGLN show that it is convenient to work with initial and final Pauli (not Dirac) spinors, $\langle 2|$ and $|1\rangle$. Photoproduction amplitudes can then be written in the form

$$\begin{aligned} \mathcal{F} = {} & i\vec{\sigma}\cdot\vec{\epsilon}\, f_1 + \frac{\vec{\sigma}\cdot\vec{q}\;\vec{\sigma}\cdot(\vec{K}\times\vec{\epsilon})}{qK} f_2 \\ & + \frac{i\vec{\sigma}\cdot\vec{K}\;\vec{q}\cdot\epsilon}{qK} f_3 + \frac{i\vec{\sigma}\cdot\vec{q}\;\vec{q}\cdot\vec{\epsilon}}{q^2} f_4 \end{aligned} \tag{38}$$

with the cross section being given by

$$\frac{d\sigma}{d\Omega} = \frac{q}{K} \langle 2|\mathcal{F}|1\rangle . \tag{39}$$

Summing and averaging over polarizations we get

$$\frac{d\sigma}{d\Omega} = q/k \left\{ |f_1|^2 + |f_2|^2 + \frac{1}{2}(1-x^2)\left[|f_3|^2 + |f_4|^2\right] - 2x\, \mathrm{Re}\, f_1^* f_2 + (1-x^2)\left[\mathrm{Re}\, f_1^* f_4 + \mathrm{Re}\, f_2^* f_3\right] + x(1-x^2)\, \mathrm{Re}\, f_3^* f_4 \right\} \tag{40}$$

where θ is the C.M. π angle and $x = \cos\theta$.

For the matrix element (37) the f's are given by

$$f_1 = \Lambda\left[-(W-M_p) + \frac{kq_0 - kq\cos\theta}{W-M}\right]$$

$$f_2 = \Lambda \frac{q}{M_p + E_p'}\left[-(W+M_p) + \frac{kq_0 - kq\cos\theta}{W-M_p}\right]$$

$$f_3 = \Lambda\, q$$

$$f_4 = \Lambda \frac{q^2}{M_p + E_p'} \tag{41}$$

where

W = total C.M. energy

θ = C.M. π^0 angle

$$\Lambda = \frac{f\, x\pi\gamma\sqrt{3}\,\gamma_{xNN}}{r_\mu r_\mu - M_x^2}\,\frac{1}{4\pi}\,\frac{W-M}{2W}\left(M_p + p_0\right)^{\frac{1}{2}}\left(M_p + p_0'\right)^{\frac{1}{2}}$$

The C.M. cross section for the pole process alone (summing and averaging over polarizations) is given by

$$\frac{d\sigma}{d\Omega} = 36\,\frac{\gamma_{xNN}^2}{4\pi}\,\frac{\Gamma(x^0 \to \pi^0 + \gamma)}{M_x^3\left(1 - \frac{\mu^2}{M_x^2}\right)^3}\,\frac{kq\,q_0^2}{r_\mu r_\mu - M_x^2} \times\left\{\beta^2 \sin^2\theta + \frac{r_\mu r_\mu}{2W^2}\left(1 - \beta\cos\theta\right)^2\right\} \tag{42}$$

where $\beta = q/q_0$ and all quantities are evaluated in the center of mass system. In the forward hemisphere the second term inside the brackets

is quite small at the energies of interest to us (< about 15% of the first term) and in fact (42) can approximately be written

$$\frac{d\sigma}{d\Omega} \approx \Gamma(\chi^0 \to \pi^0 + \gamma) \frac{\gamma_{\chi NN}^2}{4\pi} \frac{9}{M_\chi^3} \frac{\sin^2\theta}{(\cos\theta - \cos\theta_0)^2} \qquad (43)$$

where $\cos\theta_0$ is the position of the pole.

APPENDIX F. EXPERIMENTAL TESTS OF COUNTERS WITH MONO-ENERGETIC PHOTONS AND ELECTRONS

a) General

Largely to familiarize the author with the equipment, certain tests were performed using a mono-energetic source of electrons or gamma rays which was set up by Dr. Gomez and Dr. Tollestrup and other members of the spark chamber group. This source will not be described here except to say that electrons or photons were available with energies from 0 up to 1000 Mev, mono-energetic to a few percent.

The tests, which we describe here, investigated counter linearity, counter resolution, back-scattering from the counters and the degrading effects on counter energy resolution of lead in front of the counter. The first two tests had already been done by Ruderman et al. (34) and the results we obtained were in substantial agreement with theirs. Figs. 25 to 29 are supposed to be self explanatory and the rest of this appendix need not be read except for details.

b) Linearity

In Fig. 25 is shown the result of measuring the mean counter output as a function of incident electron energy. The response is essentially linear and the counter behaviour was judged to be satisfactory. The 20 Mev value of the intercept was probably due to faulty measurement of the electronic pedestal present and illustrates the sort of absolute error which can creep in even when moderate care is being taken.

c) Energy Resolution

In Fig. 26 is shown the result of measuring the relative width of the pulse height spectrum in response to mono-energetic

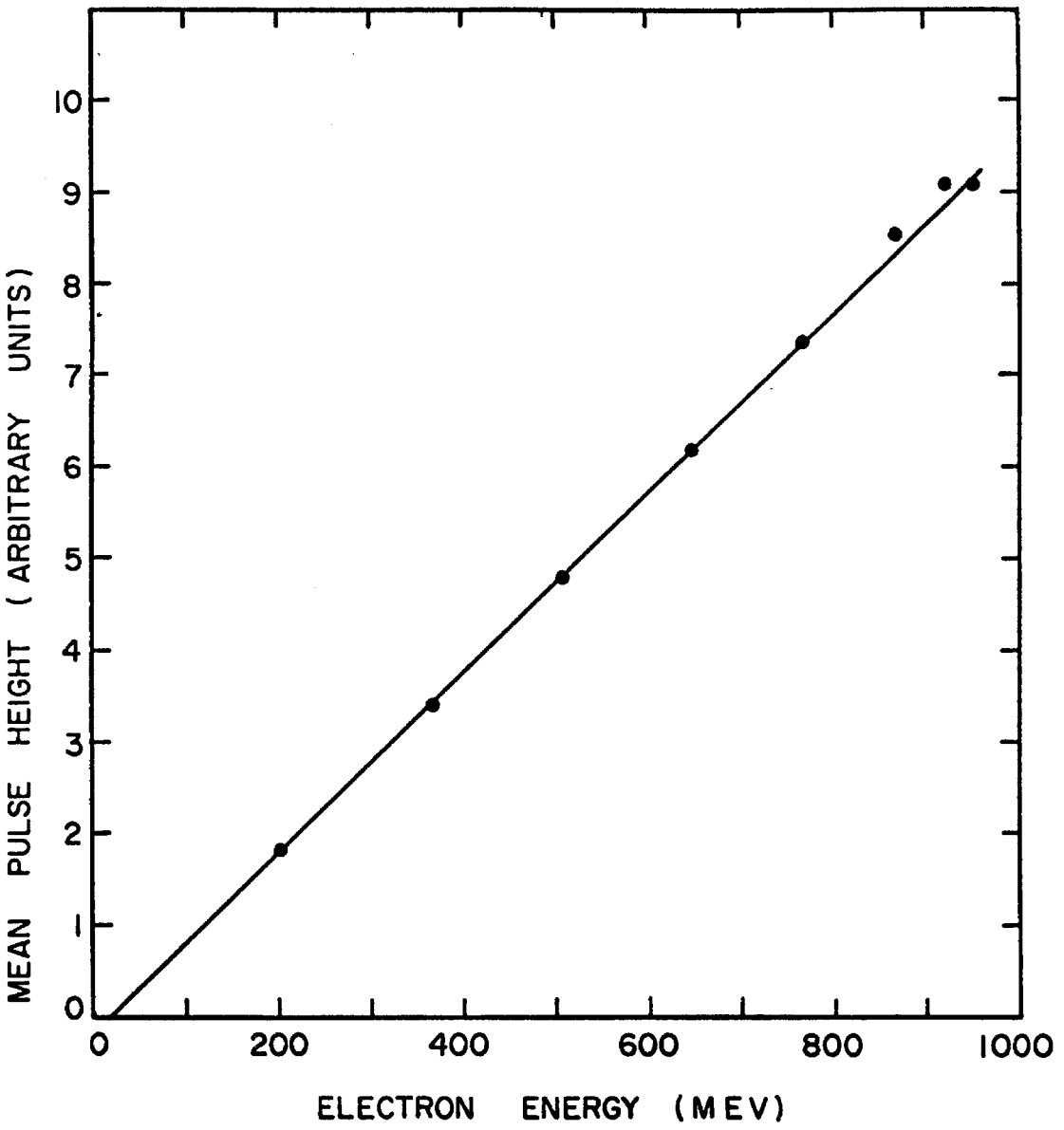

Fig. 25. Mean pulse height response of the Cerenkov counter to mono-energetic electrons.

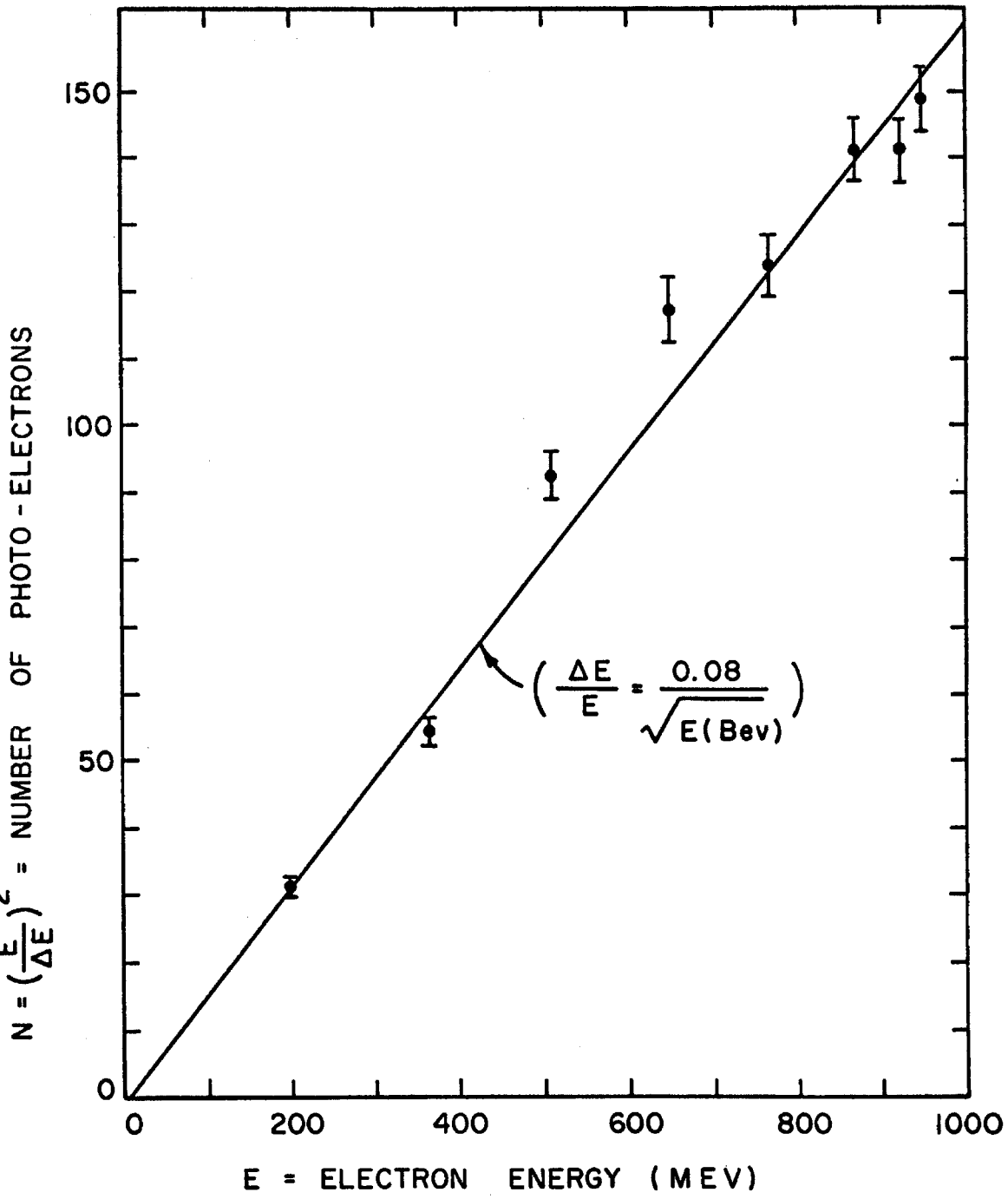

Fig. 26. ENERGY RESOLUTION. Number of photoelectrons as inferred from width of output spectrum of the pulse height response of the Cerenkov counter to mono-energetic electrons. (E = mean pulse height, ΔE = standard deviation). The errors shown are statistical and clearly underestimate the actual errors. Also the number of photo-electrons inferred in this way was probably an underestimate since the resolution function was not exactly Gaussian, having too long tails. If one fits only the peak region with a Gaussian, then one obtains the width at 1 Bev to be 6.5% instead of 8%.

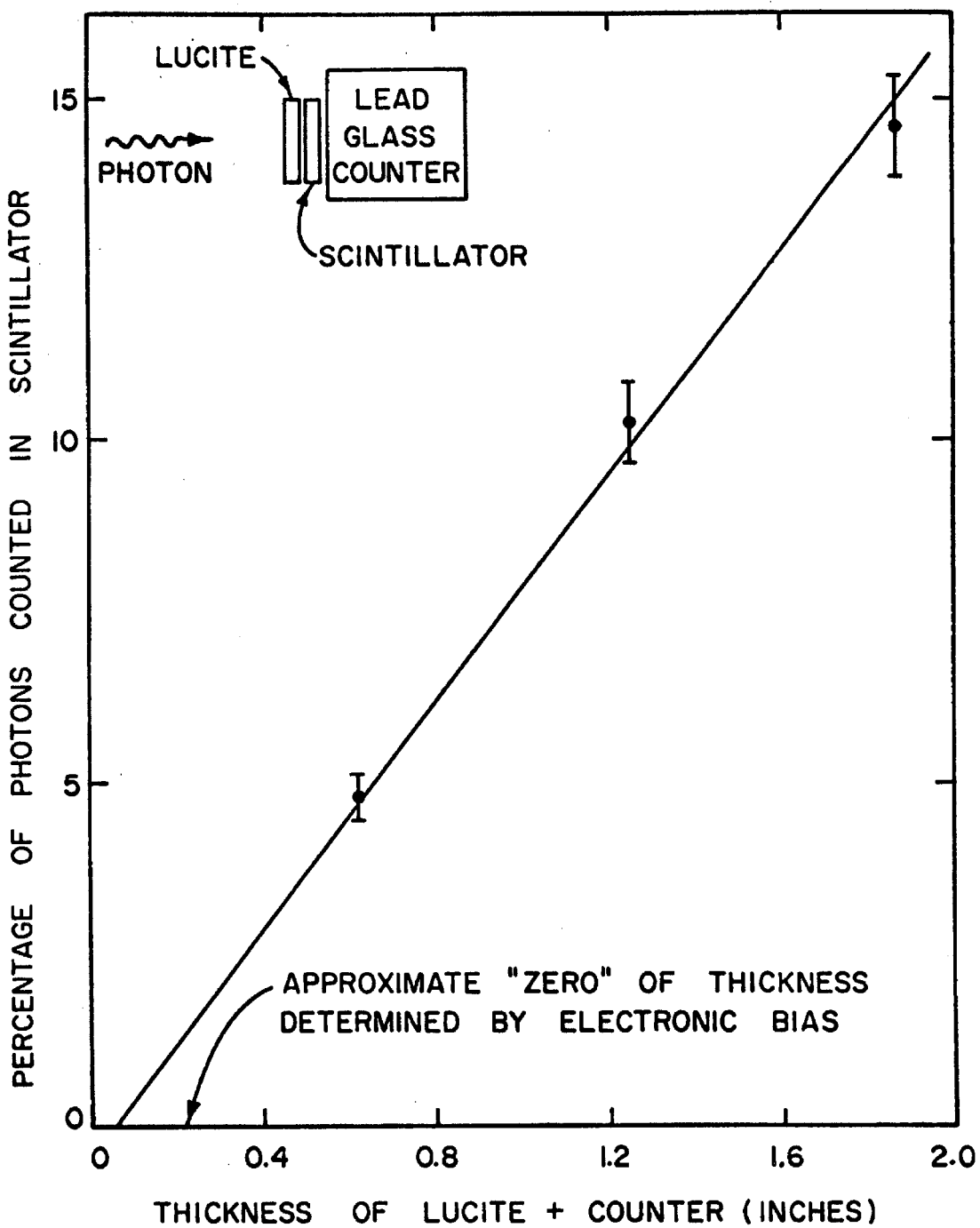

Fig. 27. BACKSCATTER. Data taken to investigate vetoing of photons due to backscatter of the shower. Counter thickness = 0.62 inches. Since this data shows this effect to have only a small probability, the effect has been consistently ignored in the rest of the thesis.

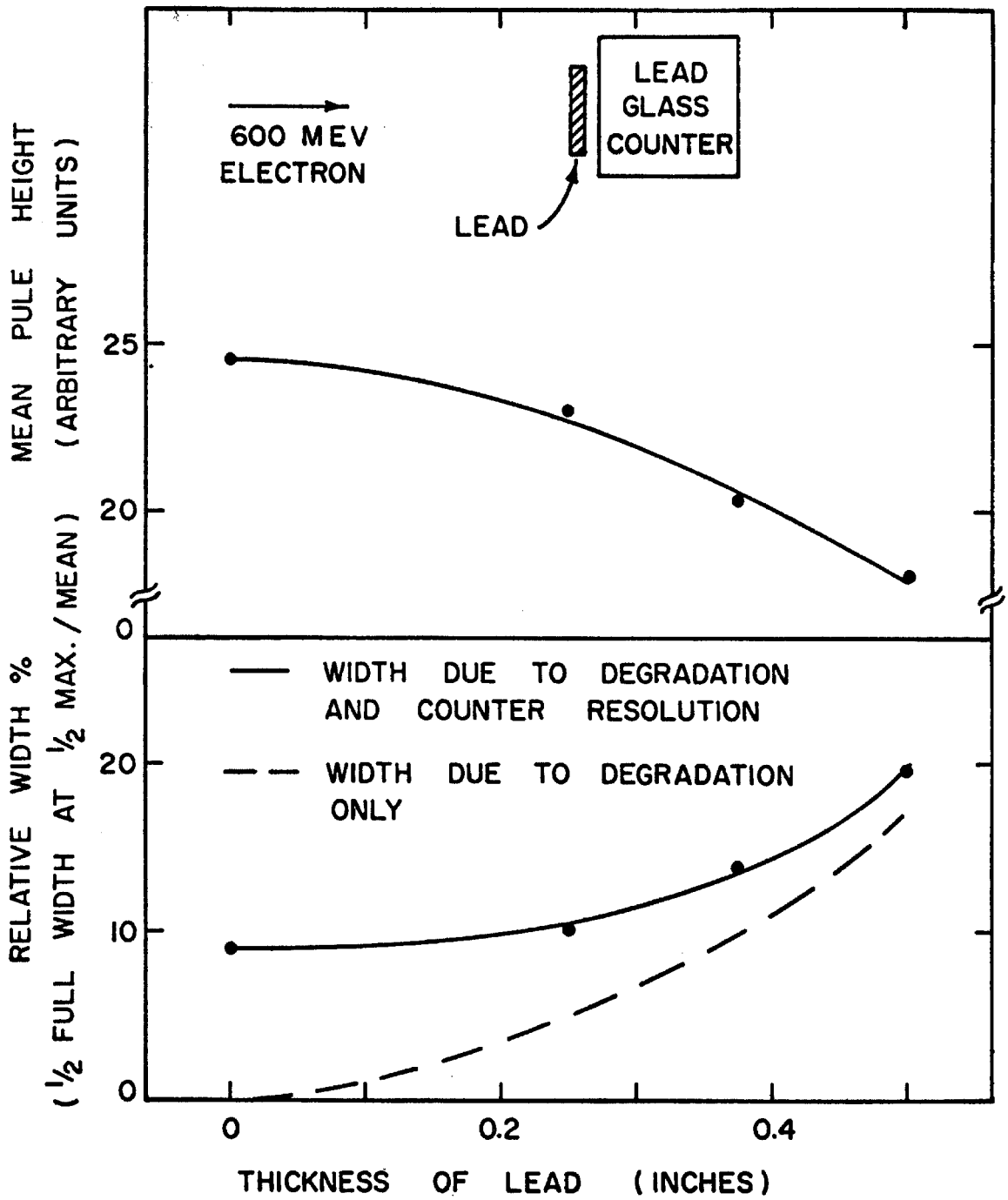

Fig. 28. ELECTRON DEGRADATION. These curves show the effect on the output of the counter of placing matter (lead) in front of the counter for incident 600 Mev electrons.

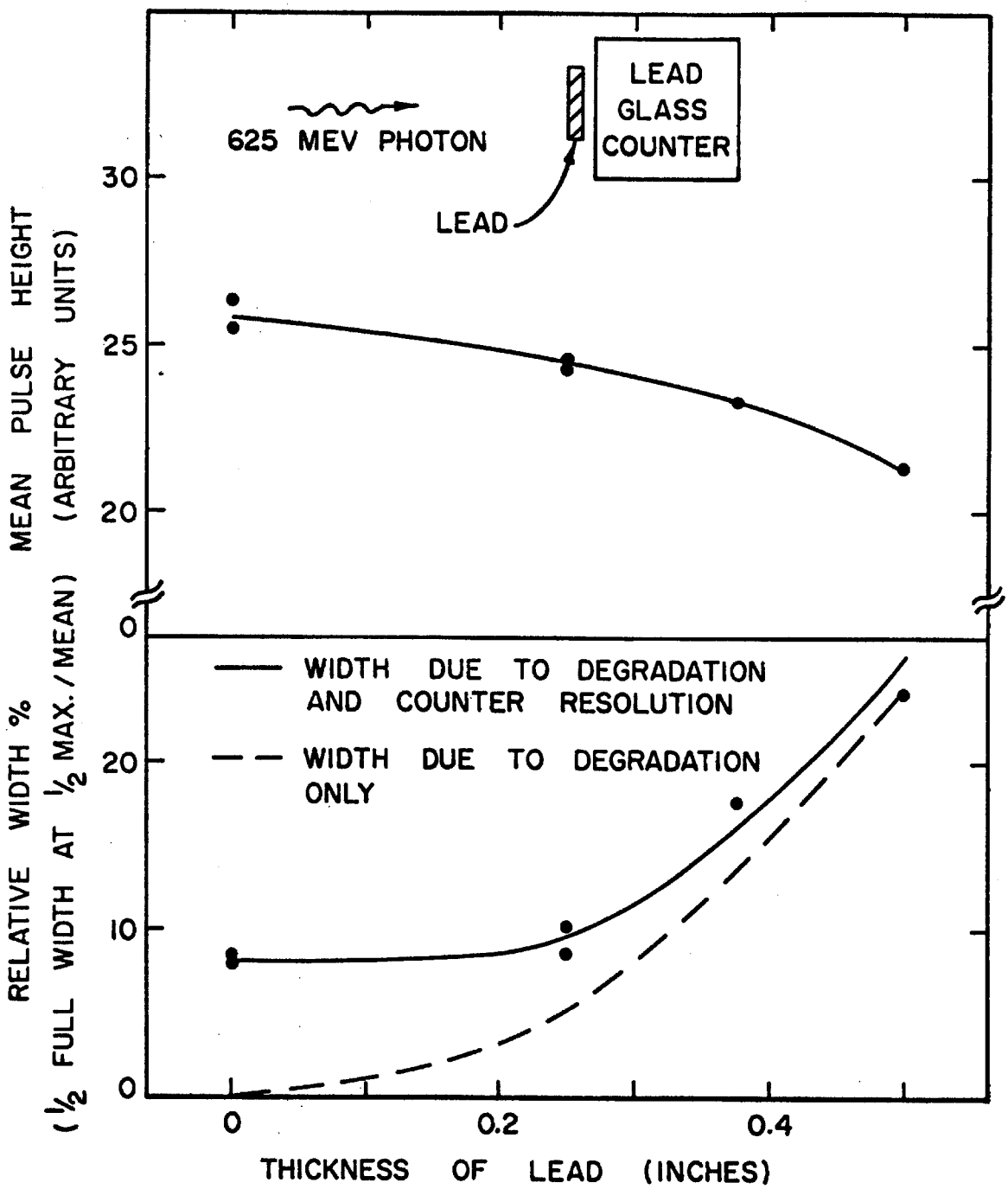

Fig. 29. PHOTON DEGRADATION. These curves show the effect on the output of the counter of placing matter (lead) in front of the counter for incident 625 Mev photons.

electrons. If ΔE is the standard deviation of the response (which is essentially Gaussian) and E is the mean, then we can ascribe all the width to photo-electron counting statistics as is shown by the linearity and the zero intercept of Fig. 26. The errors plotted in this figure are statistical. From the scatter of the points it is apparent that other errors were present, perhaps the result of electronic mishandling of pulses which varied relatively over a range of 1 to 5. The straight line fit gives $N = 160E$ (Bev) as the number of photo-electrons which corresponds to a resolution of 8% at 1 Bev. As explained in the caption to Fig. 26 this is probably an underestimate of N.

d) Back-scatter

In typical application the Cerenkov counters are used in conjunction with a scintillator as photon detectors. The scintillator requires neutral charge while the large pulse height response of the Cerenkov counter implies the shower producing capacity of the detected particle. A source of concern then is the possibility that a photon will pass through the scintillator without registering, will produce a shower in the lead glass, and then part of this shower will find its way back to the scintillator to veto the event. To investigate this effect we placed the Cerenkov counter in a 630 Mev gamma ray beam, and immediately behind a plastic scintillator. Except for the background of photons which converted in the scintillator, coincidences between the two counters could be attributed to this back-scattering process. The procedure used to eliminate this background was to run with various thicknesses of lucite in front of the scintillator and then extrapolate to "zero" scintillator thickness, i.e. to that thickness such that a pair of electrons passing through that thickness would not register

in the scintillator. The results are shown in Fig. 27. On the basis of this data, this effect was taken to be negligible.

e) Degradation of Electrons

It is frequently of interest to know what is the effect, on the energy resolution of one of the counters, of placing matter in front of the counter. In Fig. 28 is shown the mean pulse height, and the 1/2 width (at half maximum) of the spectra in the counter for various thicknesses of lead placed in front of the counter for 600 Mev incident electrons. The broken curve shows the width due to degradation in the lead only.

f) Degradation of Photons

This data is shown in Fig. 29 and is the same as in (e) above except 625 Mev photons replace 600 Mev electrons. This data would be useful in planning an experiment in which one wished to convert photons in lead but also independently to detect and measure their energy in the lead glass counter. (see Diebold et al.(10)). Perhaps more useful would be data showing the width for only those photons which actually convert in the lead. This would be useful, for example, in an experiment in which photons are counted by a scintillator behind the lead and then their energy is measured in the lead glass counter. This data was unfortunately not taken.

REFERENCES

1. B.C. Maglic, L.W. Alvarez, A.H. Rosenfeld, and M.L. Stevenson, Phys. Rev. Letters 7, 178 (1961); N.H. Xuong and G.R. Lynch, Phys. Rev. Letters 7, 327 (1961).

2. A.R. Erwin, R. March, W.D. Walker and E. West, Phys. Rev. Letters 6, 628 (1961); E. Pickup, D.K. Robinson, and E.W. Salant, Phys. Rev. Letters 7, 192 (1961). These papers contain more complete references to the earlier papers on this subject.

3. A.H. Rosenfeld, P.D. Carmony, and R.T. Van de Walle, Phys. Rev. Letters 8, 293 (1962). Further references are contained here.

4. Private communication from A.V. Tollestrup of data presented at the 1962 CERN conference.

5. M.J. Moravcsik, Phys. Rev. 125, 734(1962).

6. R.P. Feynman. 1961 Aix-en-Provence International Conference on Elementary Particles, Vol.II, p. 205

7. M.J. Moravcsik. Contained in Dispersion Relations, edited by G.R. Screaton, Oliver and Boyd, London, (1960).

8. H.Ruderman, R. Gomez, R. Talman, and A.V. Tollestrup, (to be published).

9. K. Berkelman and J.A. Waggoner, Phys. Rev. 117, 1364 (1960).

10. R. Diebold, R. Gomez, R. Talman, and R.L. Walker, Phys. Rev. Letters 7, 323(1961) and R. Diebold, private communication.

11. J.I. Vette, Phys. Rev. 111, 622 (1958).

12. J.W. DeWire, H.E. Jackson, and Raphael Littauer, Phys. Rev. 110, 1208 (1958); Phys. Rev 117, 537 (1960).

13. P.C. Stein and K.C. Rogers, Phys. Rev. 110, (1209) (1958).

14. R.M. Worlock, Phys. Rev. 117, 537 (1960).

15. H.E. Jackson, J.W. DeWire, and R.M. Littauer, Phys. Rev. 119, 1381 (1960).

16. V.L. Highland and J.W. DeWire, Bull. Am. Phys. Soc. 7, 265 (1962).

17. H.A. Bethe and F. DeHoffmann, Mesons and Fields, Row, Peterson and Co., Evanston, Illinois, (1955).

18. DeWire and Highland, private communication.

19. M. Gell-Mann, Phys. Rev. 125, 1067 (1962).

20. R.F. Peierls, Phys. Rev. 118, 325 (1960).

21. B.J. Moyer, Rev. Mod. Phys. 33, 367 (1961).

22. M. Gell-Mann and F. Zachariasen, Phys. Rev. 124, 953 (1961).

23. C. deVries, R. Hofstadter, and R. Herman, Phys. Rev. Letters, 8, 381 (1962).

24. H. Schwe, F.M. Smith, and W.H. Barkas, Bull. Am. Phys. Soc. 7, 282 (1962).

25. B.C. Maglic, L.W. Alvarez, A.H. Rosenfeld and M.L. Stevenson, Phys. Rev. Letters 7, 178 (1961).

26. Private communication from A.V. Tollestrup of data presented at the 1962 CERN conference.

27. J. Boyden, (California Institute of Technology Ph.D. thesis, unpublished).

28. R.M. Littauer, Rev. Sci. Instr. 29, 178 (1958).

29. R.R. Wilson, Rev. Sci. Instr. 29, 732 (1958).

30. J.M. Sellen, G. Cocconi, V.T. Cocconi, and E.L. Hart, Phys. Rev. 110, 779 (1958).

31. Bruno Rossi, High Energy Particles, Prentice-Hall, Englewood Cliffs, N.J. (1956).

32. S.S. Schweber, An Introduction to Relativistic Quantum Field Theory, Row, Peterson, and Co., Evanston, Illinois, (1961).

33. G.F. Chew, M.L. Goldberger, F.E. Low, and Y. Nambu, Phys. Rev. 106, 1345 (1957).

34. H. Ruderman, R. Gomez, and A.V. Tollestrup, California Institute of Technology Laboratory Report C.T.S.L.-31,(1962 unpublished).

35. M. Chretien et al. Phys. Rev. Letters 9, 127 (1962).

36. Private communication with R. Diebold.